Published in final edited form as:

*Nature*. 2017 June 15; 546(7658): 381–386. doi:10.1038/nature22405.

# ACETYL-COA SYNTHETASE REGULATES HISTONE ACETYLATION AND HIPPOCAMPAL MEMORY

**Philipp Mews**, **Greg Donahue**, **Adam M. Drake**, **Vincent Luczak**, **Ted Abel**[1], and **Shelley L. Berger**[*]

Epigenetics Institute, Departments of Cell and Developmental Biology, Biology, Genetics, University of Pennsylvania Perelman School of Medicine, Philadelphia, PA 19104, USA

## SUMMARY

Metabolic production of acetyl-CoA is linked to histone acetylation and gene regulation, yet the precise mechanisms are largely unknown. Here we show that the metabolic enzyme acetyl-CoA synthetase 2 (ACSS2) is a direct regulator of histone acetylation in neurons and of spatial memory in mammals. In a neuronal cell culture model, ACSS2 increases in nuclei of differentiating neurons and localizes to upregulated neuronal genes near elevated histone acetylation. Reduction of ACSS2 lowers nuclear acetyl-CoA levels, histone acetylation, and responsive expression of the cohort of neuronal genes. In adult mice, attenuation of hippocampal ACSS2 expression impairs long-term spatial memory, a cognitive process reliant on histone acetylation. ACSS2 reduction in hippocampus also leads to defective upregulation of memory-related neuronal genes that are pre-bound by ACSS2. These results reveal a unique connection between cellular metabolism, gene regulation, and neural plasticity, establishing a link between acetyl-CoA generation “on-site” at chromatin for histone acetylation and the transcription of critical neuronal genes.



[*]Correspondence: bergers@upenn.edu.

[1]current address: Iowa Neuroscience Institute, University of Iowa Carver College of Medicine, Iowa City, IA 52242, USA

Correspondence and requests for materials should be addressed to S.L.B. (bergers@upenn.edu).

**Online Content** Methods, along with any additional Extended Data display items and Source Data, are available in the online version of the paper.

**Data Availability** The ChIP-seq and RNA-seq data have been made available at the Gene Expression Omnibus (GEO) repository under the SuperSeries accession code GSE76854.

Animal use, surgical procedures, and all performed experiments gained IACUC approval (protocol # 804849). All personnel involved have been adequately trained and are qualified according to the Animal Welfare Act (AWA) and the Public Health Service (PHS) policy.

Supplementary Information is available in the online version of the paper

**Author Contributions** P.M. and S.L.B. conceived the project. P.M. performed most of the experiments. A.M.D. analyzed the CAD RNA-seq datasets. P.M. and G.D. performed and analyzed CAD ACSS2i and HPC RNA-seq experiments. A.M.D. and G.D. analyzed ChIP-seq datasets. P.M. and V.L. performed *in vivo* ACSS2 knockdown and behavioral characterization. P.M. and S.L.B. composed the manuscript. All authors reviewed the manuscript and discussed the work.

The authors declare no competing financial interests.

## INTRODUCTION

Memory formation involves synaptic restructuring and requires the coordinated expression of neuronal genes via poorly understood processes that modify chromatin[1,2]. Histone acetylation has emerged as a key regulator of memory storage, and restructures chromatin in distinct brain regions implicated in learning and memory, most prominently in the hippocampus[3]. Critical to hippocampal memory consolidation are the transcription factor CREB and the coactivator CREB binding protein (CBP), specifically the histone acetyltransferase (HAT) activity of CBP[4,5]. Further, inhibitors of histone deacetylases enhance memory consolidation[3]. However, comprehensive understanding of the mechanisms that regulate neuronal histone acetylation in long-term memory remains elusive.

Direct sensing of intermediary metabolites by chromatin-modifying enzymes such as acetyltransferases can dynamically adapt chromatin structure and gene expression[6,7]. Altering pools of intracellular acetyl-CoA manipulates histone acetylation[8,9], and thus, metabolic enzymes generating nuclear acetyl-CoA may directly control histone acetylation and gene expression[10,11]. In mammalian cells, there are two principal enzymes that generate acetyl-CoA for histone acetylation: acetate-dependent acetyl-CoA synthetase 2 (ACSS2) and citrate-dependent ATP-citrate lyase (ACL)[11]. The relative importance of ACSS2 vs. ACL for nuclear histone acetylation differs by tissue type, developmental state, and disease[9,11]; yet the roles for these enzymes in post-mitotic neuronal cells is unknown.

The observation that ACSS2 is highly expressed in mouse hippocampus[12] led us to investigate ACSS2 in neuronal histone acetylation and gene expression. Our findings support a critical function of neuronal ACSS2 in linking acetate metabolism to neuronal gene regulation via direct chromatin binding of ACSS2, and identify a prominent role of this mechanism in hippocampal memory consolidation.

## RESULTS

### ACSS2 regulates neuronal gene expression

We investigated a neuronal function of ACSS2 using the Cath.-a-differentiated (CAD) cell line derived from mouse catecholaminergic cells. Upon serum deprivation, CAD cells differentiate to form neuronal processes and become excitable, similar to functional neurons[13]. We examined subcellular localization by immunofluorescence, finding that endogenous ACSS2 was primarily cytoplasmic in undifferentiated CAD cells (Fig. 1a), and, upon differentiation, shifted primarily to the nucleus (Fig. 1b, Extended Data Fig. 1a). Whole cell and nuclear levels of ACSS2 increased upon CAD neuronal differentiation, contrasting with constant cytoplasmic ACL expression (Fig. 1c). In primary hippocampal and cortical neurons from mouse brain, even 14 days after isolation, ACSS2 was chiefly nuclear and ACL was primarily cytoplasmic (Extended Data Fig. 1c–f). We conclude that ACSS2, in contrast to ACL, is localized to nuclei during neuronal differentiation.

We investigated ACSS2 in upregulation of canonical neuron-specific protein markers in differentiated CAD neurons. Pre-differentiation ACSS2 knockdown (KD) lowered differentiation-linked expression of nuclear NeuN, the activity-regulated Nr4a2, and of

cytoplasmic markers Synaptophysin, Map2 and Snap25, without associated decrease of ACL (Extended Data Fig. 1g), indicating a key ACSS2 role in neuronal differentiation.

Transcriptome analysis via mRNA-seq upon CAD neuronal differentiation identified 894 upregulated genes (Extended Data Fig. 3a–c; Supplementary Table 1). Gene Ontology (GO) analysis revealed that these differentiation-linked genes are neuron specific; GO terms included neuron differentiation, synaptic transmission, ion transport, and neuron projection morphogenesis (Extended Data Fig. 3e). We built a protein interaction framework that produced a neuronal network centered on activity-dependent signaling and synaptic plasticity: Calm1 (Calmodulin 1), Grin1, and Itpr1 (Extended Data Fig. 3d). Calm1 mediates Ca2+ control of neuronal proteins in synaptic plasticity, including Ca2+/calmodulin-dependent protein kinase II (CaMKII). Such Ca2+ signaling is regulated by Grin1, an NMDA receptor subtype of glutamate-gated ion channels, and further by the ion channel Itpr1 which mobilizes intracellular Ca2+ stores, an important process in activity-dependent signaling that underlies synaptic plasticity during learning.

The metabolite acetyl-CoA is required by HAT enzymes for histone acetylation. To investigate histone acetylation during CAD neuronal differentiation, we performed chromatin immunoprecipitation-high-throughput DNA sequencing (ChIP-seq) for histone H3 lysine 9 acetylation (H3K9ac), H4K5ac, and H4K12ac (see Methods for details). All marks were enriched upon differentiation at upregulated neuronal genes, for example, at Nudix-Type Motif 1 (Nudt1) (Extended Fig. 2f). Overall, the 894 upregulated neuronal genes displayed higher acetylation compared to all other genes (Extended Data Fig. 2g).

We reduced ACSS2 or ACL using short hairpin RNAs (shRNA) prior to cell differentiation and performed RNA-seq (Extended Data Fig. 2h–k). Neuronal genes lost induction in the ACSS2 KD (pearson r = 0.15; Fig. 1d–e), while these same genes retained strong correlation in transcriptional fold change in the ACL KD (pearson r = 0.53; Extended Fig. 1l). We stratified the top 10% upregulated genes in WT cell differentiation into quintiles (Fig. 1i), revealing that ACSS2 KD strongly lowered upregulation across all quintiles (Fig. 1i: green bars; $p = 7.2*10^{-252}$, Wilcoxon rank-sum test). The ACL KD showed the same upward trend as WT, contrasting the severe defect in ACSS2 KD (Extended Data Fig. 2m; $p = 1.1*10^{-25}$, Wilcoxon rank-sum test). Of interest, the ACL KD showed lower global transcript levels (p = 1.91e-07, Mann-Whitney U test), different from the ACSS2 KD that showed a less severe defect genome-wide (Extended Data Fig. 2n, p = 0.04, Mann-Whitney U test). ACL thus has a broad but non-specific effect on gene expression, whereas ACSS2 is required for upregulation of the neuronal gene expression program upon CAD neuron differentiation.

Further, we tested the requirement for ACSS2 catalytic activity using a small molecule specific inhibitor of ACSS2 (ACSS2i)[14]. RNA-seq showed reduction of differentiation-induced genes (Fig. 1g), and the genes reduced by ACSS2 KD were also highly sensitive to the ACSS2i (Extended Data Fig. 2o, p = 1.62E-6).

## ACSS2 is recruited to transcriptionally active chromatin

We investigated direct association of ACSS2 with chromatin via ChIP-seq upon CAD neuron differentiation (see Methods for details). Two ACSS2 antibodies showed high

correlation both for MACS overlapping peaks (spearman r = 0.82; Extended Data Fig. 3a), and for global enrichment over 1kb genomic windows (spearman r = 0.73; Extended Data Fig. 3b). Binding of ACSS2 correlated with increases in histone H3K9ac, H4K5ac, and H4K12ac in differentiated relative to undifferentiated CAD neurons, for instance at promoters of Nudt1 and TAK1-Binding Protein 2 (TAB2; Extended Data Fig. 3c–d). Both genes have been linked to neurodegenerative disorders: the Nudt1 hydrolase oxidizes purine nucleoside triphosphates to prevent RNA incorporation, and TAB2 regulates signal transduction pathways in neurons[15]. Gene Ontology (GO) showed that genes proximal to ACSS2 peaks link to neuronal differentiation (Extended Data Fig. 3e). Hence chromatin-associated, neuronal gene promoter-proximal ACSS2 may provide a local source of acetyl-CoA to HAT enzymes.

We examined ACSS2 binding relative to histone acetylation, finding that 80% of ACSS2 peaks upstream of the nearest target gene overlapped an acetylation peak or have an acetylation peak downstream towards the targeted TSS (Extended Data Fig. 3f–g). A substantial number – 13–15% of all ACSS2 peaks genome-wide – directly overlapped peaks of H3 and H4 acetylation (Extended Data Fig. 3h). Also, ACSS2 peak height positively correlated overall with intersected histone acetylation peaks (Extended Data Fig. 3i–k). Peak height correlation suggests that H4 acetylation may be most responsive to ACSS2-derived acetyl-CoA, in particular H4K12ac, a mark that has been linked to defective memory formation during aging[16]. In general, the most enriched ACSS2 peaks displayed strongest histone acetylation enrichment (Extended Data Fig. 3l–n).

We investigated putative recruitment of ACSS2 via transcription factor binding using *de novo* motif discovery over ACSS2 ChIP-seq peaks, which revealed binding sequences predicted for neuronal transcription factors. The most enriched motif was Yin Yang1 (YY1) (Extended Data Fig. 3o; YY1, p = 1e-599) which recruits the two acetyl-CoA-dependent HAT enzymes CREB-binding protein (CBP) and E1A binding protein (p300)[17], consistent with ACSS2 fueling nearby catalytic HAT activity.

Initial peak analysis did not identify all ACSS2/acetylation enriched peaks (Extended Data Fig. 4a–b), hence we analyzed gene body enrichment and found additional prominent examples, such as Camk2a (Fig. 2a) encoding calcium/calmodulin-dependent protein kinase type II alpha chain, required for hippocampal long-term potentiation (LTP) and spatial learning; ACSS2/acetylation co-occupancy profiles at Camk2a were similar to Nudt1 (Extended Data Fig. 3c). Meta-gene analysis indicated that the top 5% ACSS2-enriched genes had acetylation up to three-fold higher than the mean across all genes (Extended Data Fig. 5a–d), and genes with greatest fold-change in differential ACSS2 binding had the highest histone acetylation levels (Fig. 2c; Extended Data Fig. 5e–h). GO term enrichment showed the top ACSS2-bound/acetylated genes are neuron-specific (Fig. 2b).

At all induced genes, ACSS2 binding was concomitant with increased histone acetylation (Extended Data Fig. 3p), and the 299 genes reduced upon ACSS2i treatment corresponded to the greatest gains of differentiation-linked histone acetylation (Fig. 2d). In total, about 9% of genes previously linked to neuronal differentiation (ND genes, AmiGO annotation set of 1,315 genes) were induced in the CAD cell differentiation, and these induced genes were

exceptionally sensitive to ACSS2i treatment (Fig. 2e, 'Induced' left side). Moreover, while the entire ND gene class did not change expression in CAD differentiation, they markedly lost expression upon ACSS2i treatment (Fig. 2e, 'ND' right side). We visualized the interaction between differentiation-linked gene expression changes and ACSS2 recruitment to chromatin using multiple linear regression analysis, and found a remarkable relationship between higher ACSS2 enrichment (red) and increased gene expression (Extended Data Fig. 5i). Overall, the CAD cell genomic data demonstrate dynamic ACSS2 enrichment in differentiated neurons linked to increased histone acetylation and involvement in transcriptional upregulation of neuronal genes.

## ACSS2 functions in neuronal histone acetylation

We assayed nuclear acetyl-CoA levels in the ACSS2 KD (Fig. 2f; mean $\Delta = -0.19 \pm 0.03$, $p = 0.003$) and also with ACSS2i treatment (Fig. 2f; mean $\Delta = -0.25 \pm 0.05$, $p = 0.006$), finding comparably decreased acetyl-CoA levels. This supported a role of ACSS2 enzymatic activity in supplying nuclear acetyl-CoA. Global histone acetylation levels of transcription-linked H3K27ac and H3K9ac were reduced in the ACSS2 KD (Fig. 2g, Extended Data Fig. 6a), and these are key substrates of CBP and p300 with roles in hippocampal LTP and long-term memory[18]. ACSS2 co-immunoprecipitated acetylated chromatin, specifically H3K9ac, H3K27ac, and H4K12ac (Extended Data Fig. 6b), and also CBP (Fig. 2h), suggesting a mechanism for chromatin-binding of ACSS2 at transcriptionally active genes to increase histone acetylation during memory formation *in vivo*[4,5,18].

We examined ACSS2 in primary mouse hippocampal (HPC) neurons, given their capacity for depolarization and expression of key neuronal genes functioning in memory. ACSS2 was nuclear localized (Fig. 2i), and ACSS2i treatment reduced neuronal marker expression and histone acetylation, without lowering ACSS2 levels (Fig. 2j, Extended Data Fig. 6c). ACL did not change (Fig. 2j), indicating that ACL is less important in regulation of histone acetylation in HPC neurons.

We investigated chromatin association of ACSS2 and H3K9ac *in vivo* via ChIP-seq in mouse hippocampus (HPC). Our HPC H3K9ac mapping strongly correlated with ENCODE mouse forebrain H3K9ac ChIP-seq (Spearman R = 0.67), with similar peak distribution (Extended Data Fig. 7a). HPC ACSS2 and H3K9ac corresponded genome-wide and over three canonical neuronal genes involved in memory, Arc, Egr2, and Nr2f2 (Fig. 3a–b). Additionally, ACSS2 promoter binding and H3K9ac correlated with RNA-seq in HPC (Fig. 3c). We found a small number of genes that were ACSS2-bound but not H3K9ac enriched that were silent, similar to genes not enriched for ACSS2 or H3K9ac (Fig. 3d). In contrast, genes enriched for H3K9ac were actively transcribed, but genes enriched for both ACSS2 and H3K9ac were most highly expressed (Fig. 3d).

Physical association of ACSS2/CBP in differentiated CAD cells (Fig. 2h) correlated with gene colocalization of ACSS2 and CBP in HPC, together with H3K27ac, sourcing public mouse cortex CBP and H3K27ac ChIP-seq data (ACSS2:CBP overlap p-value = 3.23e–16 by hypergeometric test). Overall, 57% of ACSS2-associated genes were co-targeted by H3K27ac (Fig. 3e), and ACSS2:CBP co-targeted genes enriched for GO terms involved in synaptic membrane potential (Extended Data Fig. 7b–c). Motif analysis at hippocampal

ACSS2 peaks show NRF1 – a transcription factor regulating neurite growth – predicted binding at 45% of ACSS2 sites (Fig. 3f), evoking an ACSS2:CBP recruitment mechanism. Moreover, ACSS2 inhibitor-sensitive genes (50%: 145/289) had proximal ACSS2 within 10kb of the TSS (hypergeometric analysis, p = 7.6986e-08), supporting a direct role for chromatin-bound ACSS2 in transcription.

## ACSS2 regulates long-term memory storage

Hippocampus-dependent spatial memory occurs through activity-dependent changes in gene expression that are coordinated, in part, through epigenetic modifications, specifically histone acetylation[19,20]. ACSS2 is expressed throughout the hippocampus (Extended Data Fig. 8a)[12,21], and thus may mediate histone acetylation to upregulate neuronal gene expression during memory consolidation[19,22]. To explore the role of ACSS2 in the adult hippocampus, we attenuated ACSS2 expression in the dorsal HPC by shRNA KD using viral vector (Fig. 4a–b). Compared to control-injected mice, ACSS2 KD animals showed similar levels in locomotion, coordination, body weight, and anxiety-related thigmotaxis during open field exploration[23] (Extended Data Fig. 8b–d; p = ns, n = 10 per group), thus, ACSS2 KD did not cause gross behavioral alterations.

To assess hippocampus-dependent spatial memory, we utilized an object-location memory paradigm[24]. Animals explore three different objects during training, and long-term memory is tested by re-exposure 24h later with one object moved to a novel location (Fig. 4a, right). In training, control and KD mice showed no difference in exploration (Fig. 4c, left). During memory retrieval, control mice displayed preferred exploration of novel location object (Fig. 4c, right, grey bar NLO2). In contrast, ACSS2 KD mice were impaired in spatial object memory (Fig. 4c, right, black bar NLO2; Extended Data Fig. 8e, mean $\Delta = -5.01 \pm 1.21$; p = 8.3e-05), and displayed a lower discrimination index (Fig. 4d; % $\Delta$DI = $-29.5 \pm 11.4$; p = 0.02). ACSS2 KD mice showed reduced total object exploration during the test (Fig. 4c, right black bars), suggesting diminished novelty associated with intact recognition of the objects from the training session (mean $\Delta = -6.13 \pm 2.15$; p = 0.02, N = 10 per group).

Previous studies have found that long-term contextual fear memory is mediated by the ventral HPC when manipulations of the dorsal HPC occur prior to training[25]. Therefore, as a control experiment, mice injected with ACSS2 KD or eGFP in the dorsal hippocampus were subjected to a contextual fear conditioning paradigm. During the 24h test session, there was no significant difference in the amount of freezing behavior between ACSS2 KD or eGFP mice (Extended Data Fig. 8f–g) suggesting a successful context-shock association mediated by the ventral hippocampus. Overall, we conclude that ACSS2 plays a critical role in dorsal HPC-mediated long-term spatial memory.

## ACSS2 regulates upregulation of immediate-early genes

Long-term spatial memory involves rapid increase of histone acetylation and immediate-early gene transcription, occurring in a sensitive time window to enable memory consolidation[19,26]; during memory retrieval, gene transcription also occurs for memory reconsolidation – which is prevented by inhibiting mRNA synthesis during the sensitive post-retrieval period[27]. We tested ACSS2 involvement in dynamic gene upregulation for

HPC memory consolidation and reconsolidation, performing mRNA-seq on the dorsal HPC. We first identified global gene expression changes induced by spatial object training, not previously investigated genome-wide. Dorsal HPC from control and shACSS2 KD mice were collected during the sensitive period of memory consolidation following spatial object training. To control for circadian oscillation, injected animals were included that had been handled but not trained.

Genes that are differentially expressed following training were discovered via transcriptome comparison of trained control injected mice to untrained circadian control injected mice using Cuffdiff. A small number of genes were induced immediately following training, featuring many known immediate-early genes, for example, Egr2, C-Fos, Nr2f2, Sgk1, and Arc (Fig. 4e; light grey bars). Importantly, baseline expression of these memory-associated genes in untrained mice was remarkably similar between control and ACSS2 KD (Extended Data Fig. 8h). In contrast, dynamic upregulation of these immediate-early genes was greatly reduced by ACSS2 KD (Fig. 4e; dark grey bars).

We further tested whether ACSS2 also regulates immediate-early gene expression in dorsal HPC during memory reconsolidation. Therefore, our HPC mRNA-seq analysis was focused on previously identified and validated genes that become upregulated following memory retrieval[26,28]. Remarkably, retrieval-associated induction of immediate-early genes did not occur during the sensitive reconsolidation period, whereas retrieval-linked downregulation during the same period was not affected by ACSS2 KD (Extended Data Fig. 9a–f).

## DISCUSSION

Metabolic state can regulate chromatin structure, prominently involving histone modifications[10]. Here, we establish a unique connection between cellular metabolism and neuronal plasticity, and reveal a neuronal function of ACSS2 as a chromatin-bound transcriptional coactivator that stimulates histone acetylation and gene expression.

Acetyl-CoA metabolism is cell and tissue specific, and is frequently dysregulated in malignant transformation[14,29]. In adipose cells, ACSS2 partially localizes to the nucleus and contributes to histone acetylation in low glucose[9,30], yet the principal metabolic determinant of histone acetylation is ACL[9]. In contrast, we show that post-mitotic neurons rely on chromatin-recruited ACSS2 to supply acetyl-CoA for histone acetylation. Of note, fasting lowers acetyl-CoA and protein acetylation in most tissues, yet acetyl-CoA levels remain unchanged in the brain[31], indicating a key role of neuronal ACSS2 in the fasted state, when acetyl-CoA production by citrate-dependent ACL is reduced.

Optimal acetyltransferase activity requires an increased local acetyl-CoA to CoA ratio, which determines catalytic activity and substrate specificity of HAT enzymes[8,9,32]. This suggests that histone acetylation is controllable via changing levels of nuclear acetyl-CoA. In this view, chromatin-bound ACSS2 could provide acetyl-CoA to fuel HAT activity locally, instantaneously recycling CoA and, further, recapture acetate from deacetylation reactions. Here, we show specific chromatin binding by ACSS2 at neuronal genes and link localization to upregulation of histone acetylation and gene transcription in spatial memory

(Fig. 4f), which requires increased histone acetylation[3,20]. We demonstrate a crucial role for ACSS2 in upregulation of immediate-early genes with key functions in neuronal plasticity and memory, leading to a critical role in long-term memory consolidation.

Epigenetic mechanisms continue to be revealed as important regulators of neural function and behavior, and are being implicated in neuropsychiatric disease, including anxiety disorders and depression[1,3,33]. In establishing ACSS2 as a key regulator at the interface of metabolic environment and neuronal chromatin, our study provides a novel enzymatic target in therapies of such neurological and cognitive disorders.

## METHODS

### Cell Culture

CAD cells (Cath.-a-differentiated; generously donated from the Holzbaur Lab at the University of Pennsylvania) were grown in DMEM:HAMS F12 (1:1), supplemented with 2mM Glutamine, 1% penicillin/streptomycin, and 10% Fetal Bovine Serum (FBS). To induce neuronal differentiation, sub-confluent CAD cell cultures (50–60%) were transferred to serum-free media (DMEM:HAMS F12 (1:1) supplemented with 2mM Glutamine) and maintained in 15 cm2 culturing dishes for 5 days. For knockdown experiments, CAD cells were infected with lentiviral hairpin constructs (TRC collection) designed against ACL (#TRCN0000055217) or ACSS2 (#TRCN0000076124, #TRCN0000076125) in medium containing 8 mg/mL polybrene and 10% FBS for 24 h. Cells then underwent selection in culture medium supplemented with 0.5 mg/mL puromycin for 5 days to obtain a stably infected population. Cell treatment with the ACSS2i (diluted in DMSO; 1-(2,3-di(thiophen-2-yl)quinoxalin-6-yl)-3-(2-methoxyethyl)urea from ChemBridge) was carried out for 24 hours total at a final concentration of 20 μm (treatment with DMSO alone served as control).

### RNA-seq

To generate libraries for RNA-seq, polyA+ RNA was extracted using the Dynabeads mRNA Direct kit (Ambion) according to the manufacturer's instructions. RNA-seq libraries for scrambled control (referred to in text as WT), shACL, and shACSS2 were made using a ScriptSeq v2 RNA-seq Library Preparation Kit from Epicentre (now Illumina). The quantity and quality of the libraries were assessed by BioAnalyzer (Agilent) and qPCR (Kapa Biosystems). The multiplexed libraries were pooled and sequenced on a single lane on the Illumina NextSeq 500 platform (50bp, single-end reads). All RNA seq data was prepared for analysis as follows: NextSeq sequencing data was demultiplexed using bcl2fastq2-v02.14.01.07. Demultiplexed FASTQs were aligned by RNA-STAR 2.3.0.e using the genome index mm10 generated from iGenome UCSC mm10 FASTQ genome sequence. The aligned reads were mapped to genomic features using cufflinks-2.2.1, (-G parameter to only quantitate known features), and iGenomes mm10 UCSC genomic transcript loci. The rRNA, mRNA, and tRNA of the mouse genome were downloaded from the goldenPath UCSC FTP and were masked from the transcript quantification. After quantification, all data processing was done using python pandas library v.0.14.0. Differential expression in CAD neurons was defined as the top 10% of genes by fold-change, corresponding roughly to 1.6-fold up-

regulation or higher. Differential expression in the inhibitor and the hippocampal ACSS2 knockdown *in vivo* were defined using Cuffdiff. The relationship between CAD cell differentiation and inhibitor function (2H) was inferred by assessing standardized scores over two RNA-seq replicates each of untreated and ACSS2i-treated cells. These were averaged and genes with $|z| < 0.5$ in either condition were dropped. Scores for remaining genes are plotted in order of increasing CAD differentiation fold change. Statistical significance of the trend and reproducibility were assessed by taking the top 20% of genes by loss of expression in the knockdown and comparing the expression of these genes in inhibitor-treated cells to a random sample of genes outside this set (Mann-Whitney test).

### Chromatin immunoprecipitation followed sequencing (ChIP-seq)

CAD cells were fixed in 1% Formaldehyde for 10 minutes and fixation was quenched with the addition of glycine to 125mM for an additional 5 minutes. Cells were harvested by scraping from plates, and washed twice in 1x PBS before storage at −80°C. ChIP was performed as previously described (Shah, P.P., et al. 2013), except that chromatin was sheared to an average size of <500 bp using the Covaris S220 Ultrasonicator. Equal aliquots of sonicated chromatin from undifferentiated and differentiated CAD neurons were used per immunoprecipitation reaction, and 10% of the amount was saved as input. ACSS2 ChIPs were performed using 2000 μg of extract and 4 μg of antibody per sample; all other ChIPs were performed using 500 μg of extract and 4 μg of antibody per sample. Immunoprecipitation was performed using protein A Dynabeads (Life Technologies). Sequencing libraries were prepared using NEBNext Ultra library preparation procedure, and then assessed for quality and quantity by BioAnalyzer (Agilent) and qPCR (Kapa Biosystems). Sequencing was performed on the Illumina NextSeq 500 platform. All ChIP-seq data was prepared for analysis as follows: NextSeq sequencing data was demultiplexed using bcl2fastq. All reads were aligned to the mm9 or the mm10 referenence genome using bowtie2.2.1. 1 alignment was allowed per read and 1 mismatch was allowed in the seed region (-N1 -k1). Reads were tabulated in fixed windows or to genes provided in the iGenome mm10 UCSC annotations using featureCounts from the subread 1.4.6 software package. CAD cell ACSS2 ChIP-seq data was normalized to input controls, while all histone acetylation ChIP-seq data was H3-subtracted. The plot in S5I is the result of performing a multiple linear regression to determine the relationship of the undifferentiated and differentiated CAD expression (regressors) and enrichment of ACSS2 in differentiated CAD cells (target). The relationship was used to color the negative space in the plot by propensity of ACSS2 binding. For the *in vivo* ChIP, hippocampal tissue pooled from two animals was finely minced and cross-linked with formaldehyde (1% final concentration) for 15 minutes at room temperature, followed by glycine quenching for an additional 10 minutes at 4°C. To create a single cell suspension, samples were washed once with ice cold PBS and homogenized by passing through a 22G needle 10 times. Subsequent steps were performed in the same way as described for the *in vitro* ChIP. *In vivo* ChIP peaks (ACSS2 (T), H3K9ac, CBP – GSM1629373, and H3K27ac – GSM1629397) were called using MACS v2.1.0 with the FDR controlled at 1%. Peak scores were assessed by adjusting to millions of aligned tags and subtracting background. Tracks were similarly normalized and are visualized using the UCSC genome browser with a maximum value windowing function and smoothing at 5 pixels (*in vitro* ChIP-seq) or using default parameters (*in vivo* ChIP-seq). The Venn diagram

in Fig. 5B shows overlap of genes (official gene symbol) that feature ChIP-seq peaks within 1kb of their nearest TSS. Venn diagrams in Fig. 5E and S6B display overlapping target gene sets (RefSeq transcripts) that were assigned to the entire set of ChIP-seq peaks, since CBP binds to few genes within 1kb of the TSS. The *in vivo* mRNA expression vs. ChIP analysis (Fig. 5C) was created by sorting genes on log2 transformed expression values (DESeq library-size adjusted, replicate-averaged values) in home cage control mice then displaying ChIP-seq AUCs (RPM-adjusted ChIP minus RPM-adjusted background, length adjusted) for each gene for the peak closest to its TSS within a distance of 1kb (all genes with more distal peaks were rendered as having a score of zero). Gene targets were inferred by the presence of peaks proximal to the TSS (within 1kb). To identify enriched motifs (Fig. 5F), *in vivo* ACSS2 peaks targeting genes up-regulated in differentiated CAD cells (without respect for distance to the nearest TSS) were compared to a background set of equal-sized regions selected from gene-rich regions using HOMER (peak sizes were fixed at 300bp). Discovered motifs were filtered for those present at 1/3 or more of the targeting peaks and with a 10-fold or higher enrichment over the gene-rich background. To assess the overlap of in ACSS2 and histone acetylation (Fig. 3E, S3D), ACSS2 peaks were filtered to include only those upstream of their nearest target genes. Downstream acetylation was assessed for similarly filtered peaks of H3K9ac, H4K5ac, and H4K12ac from the same cells, as well as cortical H3K27ac. For the in vivo analysis (5B), gene targets of ACSS2 or H3K9ac peaks within 1kb of their nearest TSS were examined for overlap. The acetylation pattern due to differentiation at induced or inhibitor-sensitive genes (Fig. 3J, 3K) was assessed by taking a 20kb window around the TSS and measuring input-adjusted ChIP-seq signal. H3K9ac data were validated (Extended Data Fig. 6A) by comparing to ENCODE's common-replicate peaks for H3K9ac in mouse forebrain (accession ENCSR369RBO) using CEAS (default parameters, with a 1kb–10kb window around the TSS and TES). Additional comparisons were made to H3K9ac (NCBI GEO: GSE82643) and H3K27ac (GSE82428), contrasting to input (GSE82659) to control for sonication efficiency. Cortical H3K27ac (NCBI GEO: GSM1629397) and CBP (GSM1629373) were aligned along with the corresponding input (GSM1629381) using bowtie2 (parameters -k 1 -N 1 --local) and peaks were called using MACS2 (input control, FDR controlled at 1%) (Fig. 5E, S6B). The combined effect of ACSS2 and histone acetylation targeting on gene expression in vivo (Fig. 5D) was demonstrated by box-plotting expression in home cage control mice at genes targeted by ACSS2 by itself, H3K9ac by itself, ACSS2 + H3K9ac, or neither. Only genes bound at the promoter (1kb distance) by ACSS2 were considered.

### Acetyl-CoA Quantification

To extract and quantify acetyl-CoA in differentiated CAD neurons, $4 \times 10^6$ cells were washed and incubated in lysis buffer for 30 minutes (10 mM Tris pH 8, 1 mM KCl, 1.5 mM MgCl2, 1 mM DTT). The nuclei were pelleted at 3000g for 5 minutes, and immediately re-suspended in Acetyl CoA Assay Buffer provided in the PicoProbe Acetyl CoA Assay Kit available from Abcam (ab87546). The acetyl-CoA assay, including the deproteinization step, was prepared per instructions by the manufacturer. The PicoProbe assay was performed in 96 well clear-bottom plates, and the resulting fluorescence was quantified using the Synergy™ HTX Multi-Mode Microplate Reader (BioTek Instruments).

### Western blots

Cells were lysed in buffer containing 50mM Tris pH 8.0, 0.5mM EDTA, 150mM NaCl, 1% NP40, 1% SDS, supplemented with protease inhibitor cocktail (Life Technologies, #78446). For subcellular fractionation experiments, the cells were processed using the subcellular fractionation kit for cultured cells (Thermo Scientific 78840) according to the manufacturer instructions. Protein concentration was determined by BCA protein assay (Life Technologies, number 23227), and equal amounts of protein were used in co-immunoprecipitation experiments or directly loaded on polyacrylamide gels. The endogenous co-immunoprecipitation (co-IP) experiments were performed using antibody-conjugated protein A Dynabeads (Life Technologies) in buffer containing: 20 mM Tris, pH 8.0, 137 mM NaCl, 1 mM $MgCl_2$, 1 mM $CaCl_2$, 1% NP-40, 10% glycerol, with protease and phosphatase inhibitors, and 12.5 U $ml^{-1}$benzonase (Novagen, 70746). Proteins or co-IP eluates were loaded and separated on 4–12% Bis-Tris polyacrylamide gels (NuPAGE). After transfer to nitrocellulose membrane, 3% BSA in TBS supplemented with 0.1% Tween 20 (TBST) was used to block the membrane at room temperature for 1 hour. Primary antibodies were diluted in TBST, and incubated at 4°C overnight. Primary antibodies are listed below. The membrane was washed 3 times with TBST, each for 10 minutes, followed by incubation with HRP-conjugated secondary antibodies at room temperature for 1 hour, in TBST. The membrane was washed again 3 times, and imaged by Fujifilm LAS-4000 imager. Original gel blots provided as Supplementary Figure 1.

### Immunofluorescence

Cells were fixed in 4% PFA in PBS for 20 minutes at room temperature. Cells were washed twice with PBS, and permeabilized with 0.5% Triton X-100 in PBS for 10 minutes. After washing two times, cells were blocked in 10% BSA in PBS for 1 hour at room temperature. Cells were incubated with primary antibodies in 5% BSA in PBS supplemented with 0.1% Tween 20 (PBST) overnight at 4°C. Antibodies are listed below. Then cells were washed four times with PBST, each for 10 minutes, followed by incubation with fluorophore-conjugated secondary antibody in 5% BSA in PBST for 1 hour at room temperature. F-actin was labeled using Alexa Fluor® 488 Phalloidin (Thermo A12379). Cells were then washed three times in PBST, once with PBS, and incubated with 1 μg/ml of DAPI for 5 minutes. The cells were then washed twice with PBS, and mounted with ProLong Gold (Invitrogen). The slides were observed and imaged using a Nikon Eclipse microscope. Microscopy settings were unchanged between samples.

### Antibodies

Antibodies included Anti-H3 (Abcam ab1791), Anti-H3K9ac (Abcam ab4441), Anti-H3K27ac (Abcam ab4729), Anti-H3K122ac (Abcam ab33308), Anti-H4 (Millipore 05-858), Anti-H4K5ac (Millipore 39-584), Anti-H4K12ac (Abcam ab1761), Anti-ACSS2 (T) (Thermo MA5-145810), Anti-ACSS2 (CS) (Cell Signaling 3658), Anti-ACL (Proteintech 15421-1-AP), Anti-α-Tubulin (Sigma T8328), Anti-GAPDH (Fitzgerald Industries 10R-G109A), Anti-KAT3A/CBP (Abcam ab2832), Anti-SNAP25 (Abcam ab5666), Anti-Synaptophysin (Millipore MAB368), Anti-MAP2 C/D (Cell Signaling #8707), Anti-NR4A2 (Santa Cruz sc-991), Anti-NeuN (Millipore ABN78)

### Intracranial injection of viral vector

Adult mice (8+ weeks of age) were anesthetized with isoflurane gas (1–5% to maintain surgical plane) and placed in a sterile field within a stereotaxic device. Animals received an injection of bupivacaine (2.5mg/Kg) for local anesthesia before the skin was disinfected with betadine solution and the skull exposed with a short incision using sterile surgical equipment. Artificial tears were applied to eyes to ensure sufficient lubricating. A small hole (about 0.5 millimeters) was be drilled in the skull over the target area using a stereotax and a stereotactic drill. A micro-syringe filled with viral vector was inserted into the dorsal hippocampus and slowly removed following injection (AP, −2.0mm; DV, −1.4mm; ML, +/−1.5mm from Bregma; AAV2/9.U6.shACSS2.CMV.EGFP = ACSS2 knockdown vector; AAV2/9.CMV.EGFP.polyA = eGFP-control vector). All animals received a single dose of subcutaneous meloxicam (5 mg/kg) as analgesia (pain medicine) at induction and one dose per day for two days post-operatively as needed.

### Object location memory (OLM) task

The OLM procedure is used to test spatial memory. The procedure consists of a training phase and a testing phase. Prior to training, each mouse was handled for 3 minutes a day for 3 days. During the training day, mice are placed in an arena (approx. 1 square foot) containing 3 different objects. The objects used were a glass bottle, a metal tower (5H × 2W × 2L inches), and a plastic cylinder. Mice were habituated to an empty arena with a black and white striped spatial cue on the wall, followed by object exposure in three 6 minute trials with and interval of 3 minutes. The arena and objects were cleaned with 70% EtOH between trials. To diminish biases, the memory test was performed on control and KD mice on the same day in the same arena, using every combination of object location (n = 10 mice per study group). After 24 hours, the individual mice were placed back in the arena used in the testing phase. For testing, one of the objects was moved to different location in the arena. Mice were allowed to freely explore for 5 minutes. Each session was recorded using a video camera and time spent exploring (approaches and sniffing) each object was assessed offline.

### Contextual fear conditioning

The animal was placed in the conditioning chamber (Med Associates) for 5 min before the onset of the unconditioned stimulus (US), a 1.5 mA of continuous foot shock. A mild 2 sec., 1.5 mA foot shock is used as an aversive stimulus, which does not injure the mice in any way but provides the transient, yet startling and aversive, stimulus that is necessary for conditioning. After an additional 30 s in the chamber, the mouse was returned to its home cage. Twenty-four hours later, the mouse was tested for a freezing response to the chamber (contextual) where training occurred. Time spent freezing in the chamber (motionless except for respiratory movements) in the chamber was assessed for 5 consecutive minutes.

## Extended Data

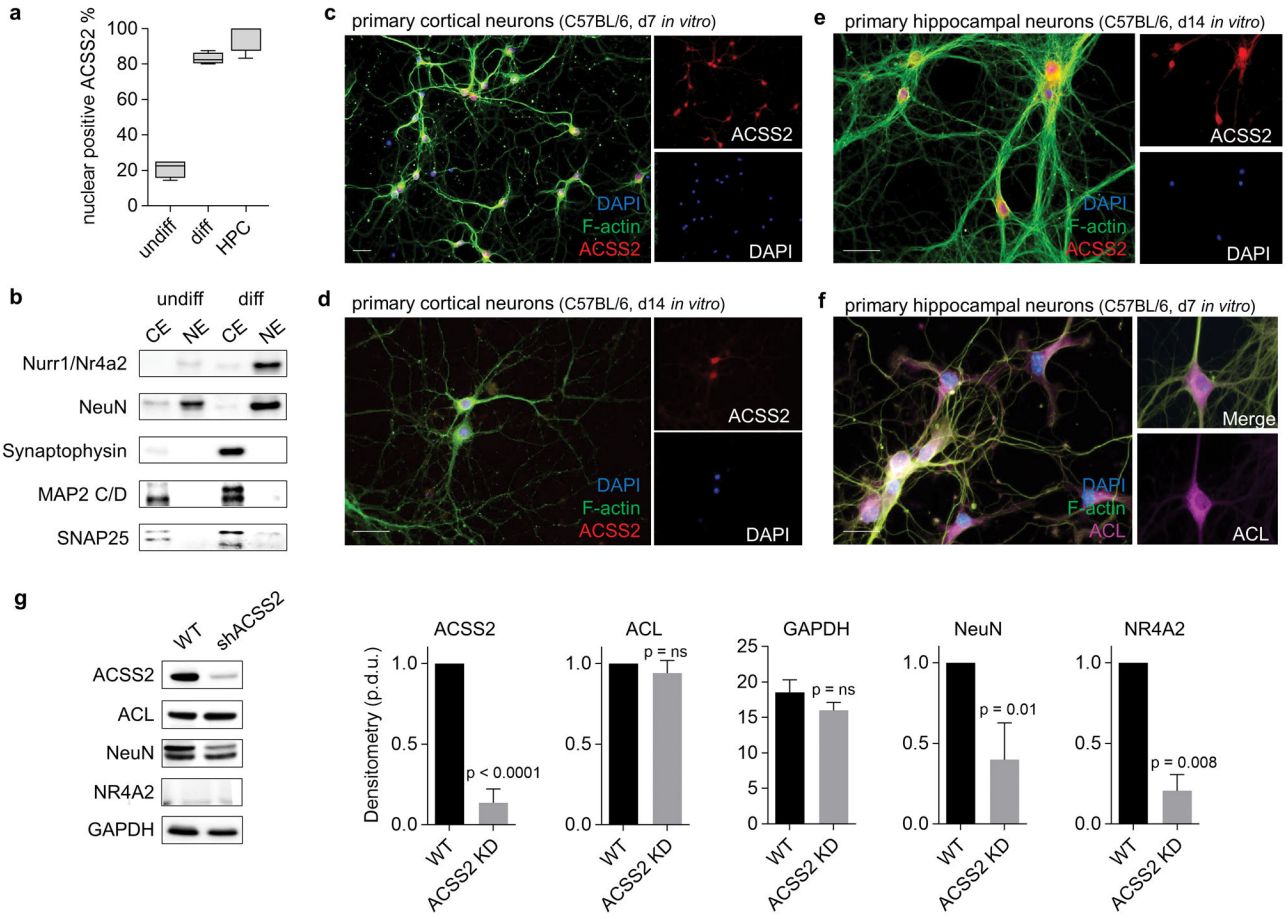


**Extended Data Figure 1.**

ACSS2 localizes to the nucleus of neurons. (a) Shown is the percentage of cells with nuclear staining in ACSS2 immunofluorescence experiments (undiff – undifferentiated CAD cells, diff – differentiated CAD neurons, HPC – primary hippocampal neurons day 7; examined were a minimum of 50 cells in three replicate IF; T test undiff vs diff $p < 0.0001$, undiff vs HPC $p < 0.0001$, error bars: SE) (b) Western blots of cytoplasmic (CE) and nuclear (NE) extracts from undifferentiated CAD cells and differentiated CAD neurons were probed with the indicated antibodies. (c, d) Immunofluorescence in primary cortical neurons isolated from C57BL/6 embryos, at day 7 (c) and day 14 (d) of *in vitro* differentiation culture. ACSS2 locates predominantly to nuclei in differentiated primary cortical neurons. Scale bar = 25 μm (e) Immunofluorescence in primary hippocampal neurons isolated from C57BL/6 embryos at day 14 of *in vitro* differentiation culture. ACSS2 locates predominantly to nuclei in differentiated primary neurons. Scale bar = 25 μm (f) Immunofluorescence in primary hippocampal neurons at day 7 shows that ACL is chiefly localized to the cytoplasm of primary hippocampal neurons. Scale bar = 25 μm (g) Neuronal differentiation markers decrease in ACSS2 knockdown. CAD cells were infected with lentiviral control (WT) or knockdown vector (shACSS2). Western blots of lysates from stably infected differentiated

cells were probed with the indicated antibodies, and quantified using ImageJ (n = 3, error bars: SE).

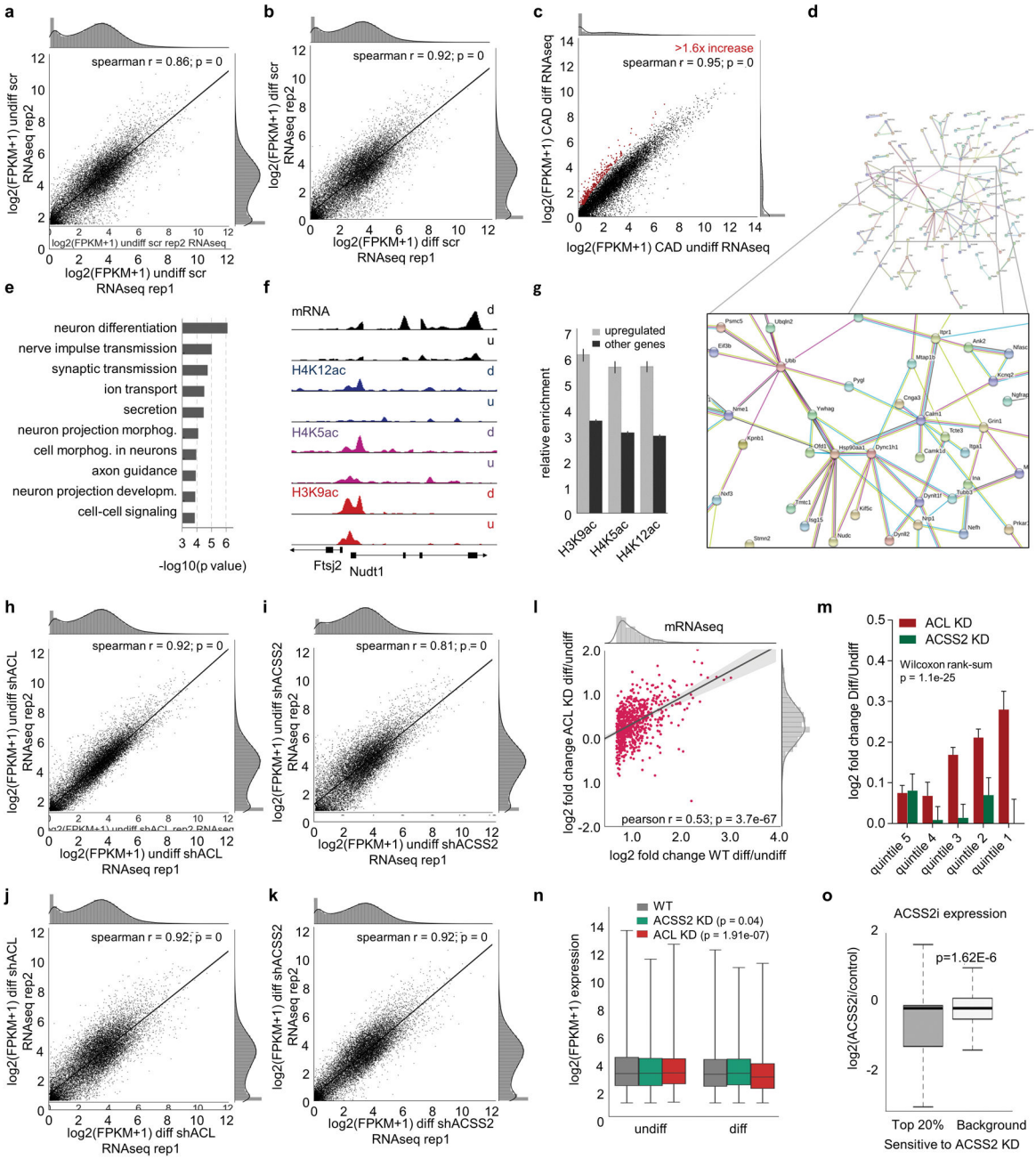


**Extended Data Figure 2.**

(a–b) Correlation plots of replicate RNA-seq in (a) undifferentiated CAD cells and (b) differentiated CAD neurons for scramble control (spearman r = 0.86, p = 0; and spearman r = 0.92, p = 0). (c) Transcriptome analysis via RNA-seq, done in two highly correlated biological replicates, identified 894 genes that become upregulated in differentiated CAD neurons (red dots depict genes with >1.6-fold increase, spearman r = 0.95, p = 0). (d)

Pathway analysis of the 894 upregulated genes (red dots in Fig. 2a) using StringDB. Shown is the protein-protein interaction graph depicting a network of binding partners that centers on key players of activity-dependent signaling and synaptic plasticity: Itpr1, Grin1, Nefh, Dync1h1, and Calm1. (e) Gene ontology (GO) enrichment analysis shows upregulation of neuronal pathways. GO was employed on the 894 genes that become upregulated in differentiated CAD neurons (Extended Data Fig. 2c; identified by RNA-seq, FE > 3.5, FDR < 0.005). (f) Genome browser view of Nudt from RNA-seq and ChIP-seq (H4K12ac, H4K5ac, and H3K9ac: mm10 chr5: 140,327,500–140,339,000). (g) Bar plot shows the relative genic enrichment of H3K9ac, H4K5ac, and H4K12ac at genes that are upregulated in the CAD neuron differentiation (>1.6-fold, grey bars) versus all other genes (black bars). (h–i) Correlation plots of replicate RNA-seq in undifferentiated CAD cells for ACL knockdown (h; spearman r = 0.92, p = 0), and ACSS2 knockdown (i; spearman r = 0.81, p = 0). (j–k) Correlation plots of replicate RNA-seq in differentiated CAD neurons for ACL knockdown (j; spearman r = 0.92, p = 0), and ACSS2 knockdown (k; spearman r = 0.92, p = 0). (l) ACL KD has much lower effect on differentiation-linked upregulation of neuronal gene expression program (compare to Fig. 1d). Scatter plot contrasts the fold-change FPKM of induced genes (Extended Data Fig. 2c) between WT and ACL KD (pearson r = 0.53, p = 3.7e-67). Marginal distributions show histogram and kernel density estimation. Ordinary least squares linear regression is displayed with 95% confidence interval. (m) Shown are the corresponding quintiles of upregulated genes (red dots in Extended Fig. 2c) with the greatest fold-change FPKM increase in WT. The ACL KD showed the same upward trend as WT (red bars, compared to WT black bars in Fig. 1f), contrasting the severe defect in ACSS2 KD (green bars; (for each quintile, columns represent the mean induction value of genes, p = 1.1*10–25, Wilcoxon rank-sum test, error bars: SE). (n) Boxplot of global mRNA transcript levels in undifferentiated (undiff) and differentiated (diff) CAD neurons from RNA-seq in WT (scramble control knockdown; grey), ACSS2 KD (shACSS2 #25 knockdown; green), and ACL KD (shACL #17 knockdown; red). Genome-wide transcript levels are reduced in diff ACL KD when compared to diff WT (p = 1.91e-07, Mann-Whitney U test, error bars: SE), whereas global reduction in diff ACSS2 KD is less significant when compared to diff WT (p = 0.04, Mann-Whitney U test, error bars: SD). (o) Genes sensitive to ACSS2 KD (top 20%) are also sensitive to the ACSS2i treatment, which lowers their expression compared to all genes (p = 1.62E-6, SD).

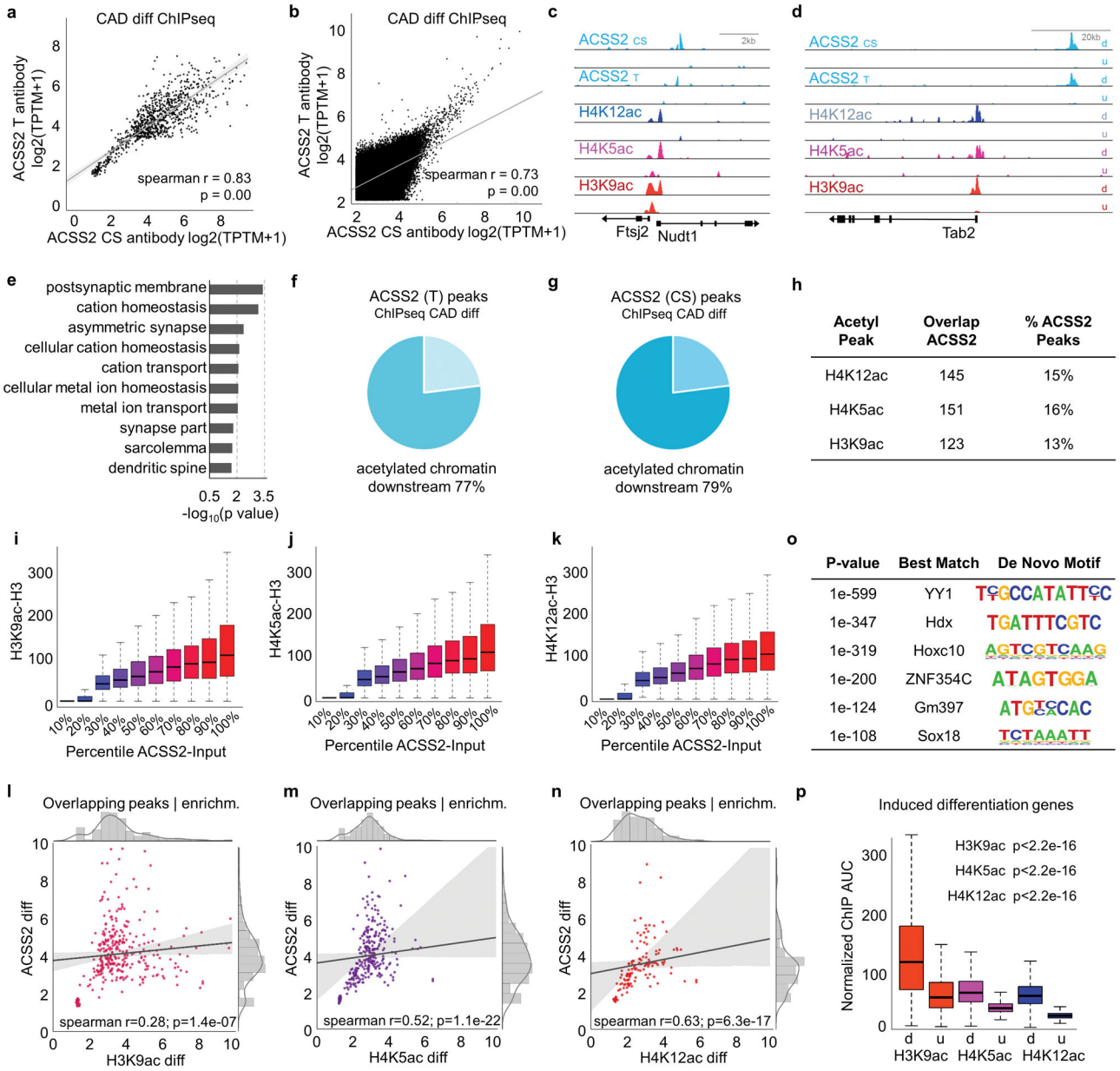


| Acetyl Peak | Overlap ACSS2 | % ACSS2 Peaks |
|---|---|---|
| H4K12ac | 145 | 15% |
| H4K5ac | 151 | 16% |
| H3K9ac | 123 | 13% |

| P-value | Best Match | De Novo Motif |
|---|---|---|
| 1e-599 | YY1 | TCGCCATATTCC |
| 1e-347 | Hdx | TGATTTCGTC |
| 1e-319 | Hoxc10 | AGTCGTCAAG |
| 1e-200 | ZNF354C | ATAGTGGA |
| 1e-124 | Gm397 | ATGTCCAC |
| 1e-108 | Sox18 | TCTAAATT |

**Extended Data Figure 3.**

ACSS2 is chromatin-bound in differentiated CAD neurons (a) ChIP-seq in differentiated CAD neurons was performed in replicate with two different antibodies to ACSS2. Correlation plot displays relative enrichment over corresponding MACS peaks (default parameters with Input as control, 1598 peaks). (b) Correlation plot displays relative ChIP-seq enrichment genome-wide. (c) UCSC Genome Browser views of ChIP-seq tracks show that, upon CAD neuron differentiation, increases in H4K5, H4K12, and H3K9 acetylation over the NUDT1 gene locus co-occur with ACSS2 enrichment (U–undiff, D–diff; chr5: 140,326,845–140,339,655). (d) UCSC Genome Browser view of indicated ChIP-seq tracks in undifferentiated CAD cells (u) and differentiated CAD neurons (d) over Tab2 locus (chr10: 7,875,000–8,004,000). (e) GO enrichment analysis of the genes most proximate to

ACSS2 peaks demonstrates that neuron-specific genes are enriched. (f) Frequency of ACSS2 peaks (T antibody) located upstream of their target gene associated with histone acetylation. (g) Frequency of ACSS2 peaks (CS antibody) located upstream of their target gene associated with histone acetylation. (h) Table shows % direct overlap of ACSS2 peaks with H3K9ac, H4K5ac, and H4K12ac broad MACS peaks. (i–k) Decile plots depict enrichment of H3K9ac (i), H4K5ac (j), and H4K12ac (k) over ranked deciles of ACSS2 peak enrichment (zeroes removed). (l–m) Differentiation-induced co-enrichment of ACSS2 and acetyl broad peaks (MACS). Peak enrichment correlation indicated for H3K9ac (i; spearman r = 0.28, p = 1.4e-07), H4K5ac (m; spearman r = 0.52, p = 1.1e-22), and H4K12ac (n; spearman r = 0.63, p = 6.3e–17). (o) Discovered *de novo* motifs for transcription factor binding sites predicted by HOMER from all ACSS2 ChIP-seq peaks called by MACS in differentiated CAD neurons. (p) ChIP-seq enrichment of differentiation-induced genes as a group show correlation with histone acetylation in differentiated CAD neurons.

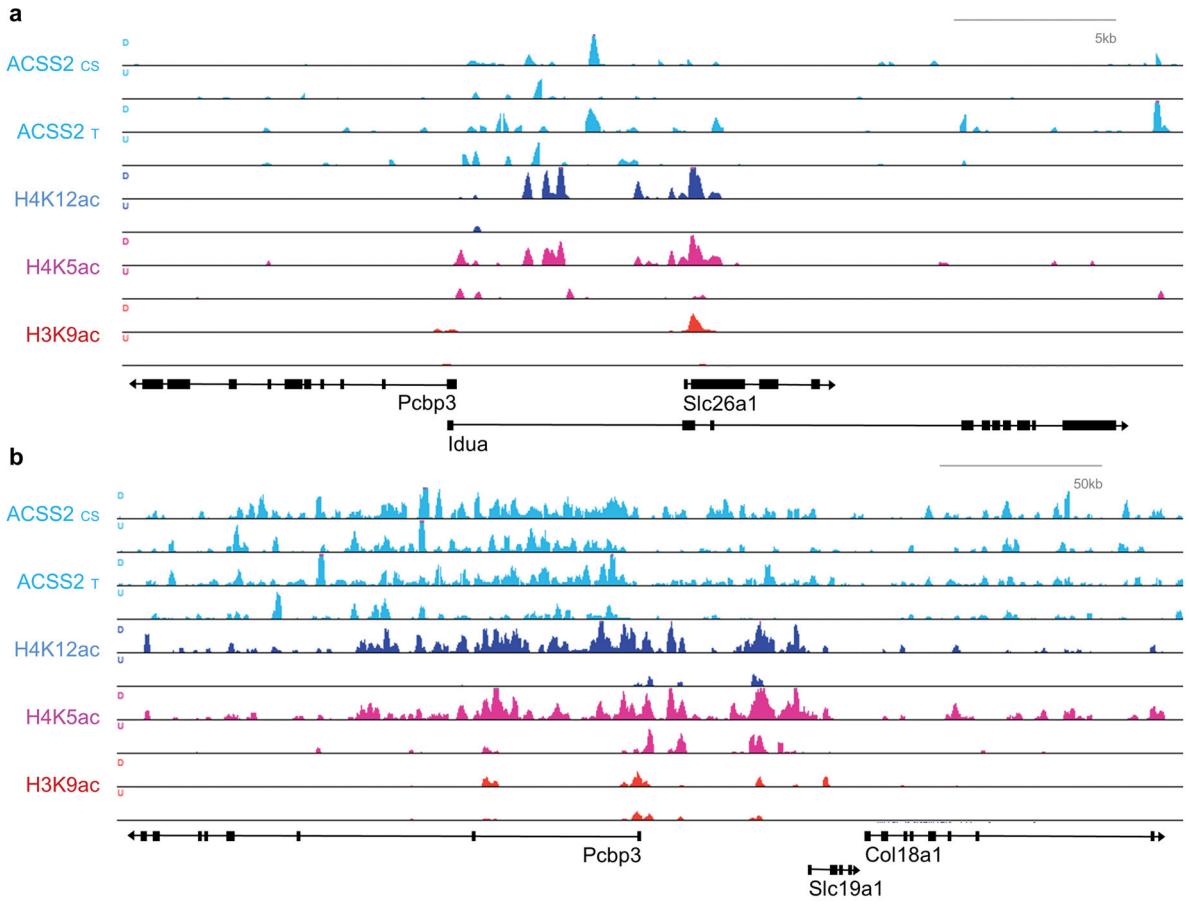


**Extended Data Figure 4.**

(a) UCSC Genome Browser views of ChIP-seq tracks demonstrate that increases in H4K5, H4K12, and H3K9 acetylation co-occur with ACSS2 enrichment over the Idua (Alpha-L-iduronidase) gene locus upon CAD neuron differentiation (U–undiff, D–diff; chr5: 108,649,457–108,687,261). (b) At the *Slc19A1* (Solute Carrier Family 19 – Folate Transporter – Member 1) gene, elevated histone H4K5, H4K12, and H3K9 acetylation levels

correspond with increasing ACSS2 enrichment in CAD neuron differentiation (chr10: 76,761,141–77,170,455).

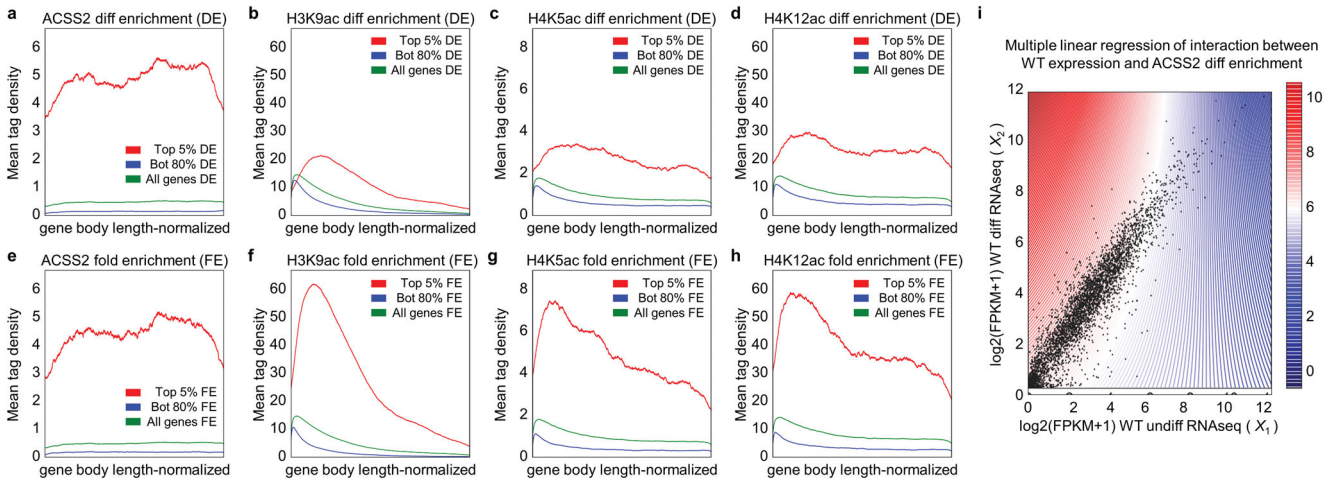


**Extended Data Figure 5.**

(a–d) Meta-gene enrichment analysis shows ChIP occupancy for ACSS2 (a), H3K9ac (b), H4K5ac (c), and for H4K12ac (d) across the top 5% of genes enriched for ACSS2 in differentiated CAD neurons (Top 5% DE; red). The bottom 80% of genes (Bot 80% DE) is shown in blue, and the average signal across all genes (All genes DE) is shown in green. (e–h) Meta-gene enrichment analysis shows ChIP occupancy for ACSS2 (e), H3K9ac (f), H4K5ac (g), and for H4K12ac (h) at the top 5% of genes that become dynamically bound by ACSS2 upon neuronal differentiation (Top 5% DE; red). The bottom 80% of genes (Bot 80% DE) is shown in blue, and the average signal across all genes (All genes DE) is shown in green. (i) Multiple linear regression analysis was implemented to model the interaction between genic ACSS2 enrichment and WT gene expression changes, and to visualize the interaction between differentiation-linked gene expression changes and ACSS2 recruitment to chromatin. The contour plot of this fitted regression model displays high levels of ACSS2 enrichment in red and low levels in blue, and is overlaid with the scatter plot of the independent gene expression variables. The visualized model demonstrates that high ACSS2 enrichment (red) corresponds to increased gene expression in the CAD neuronal differentiation.

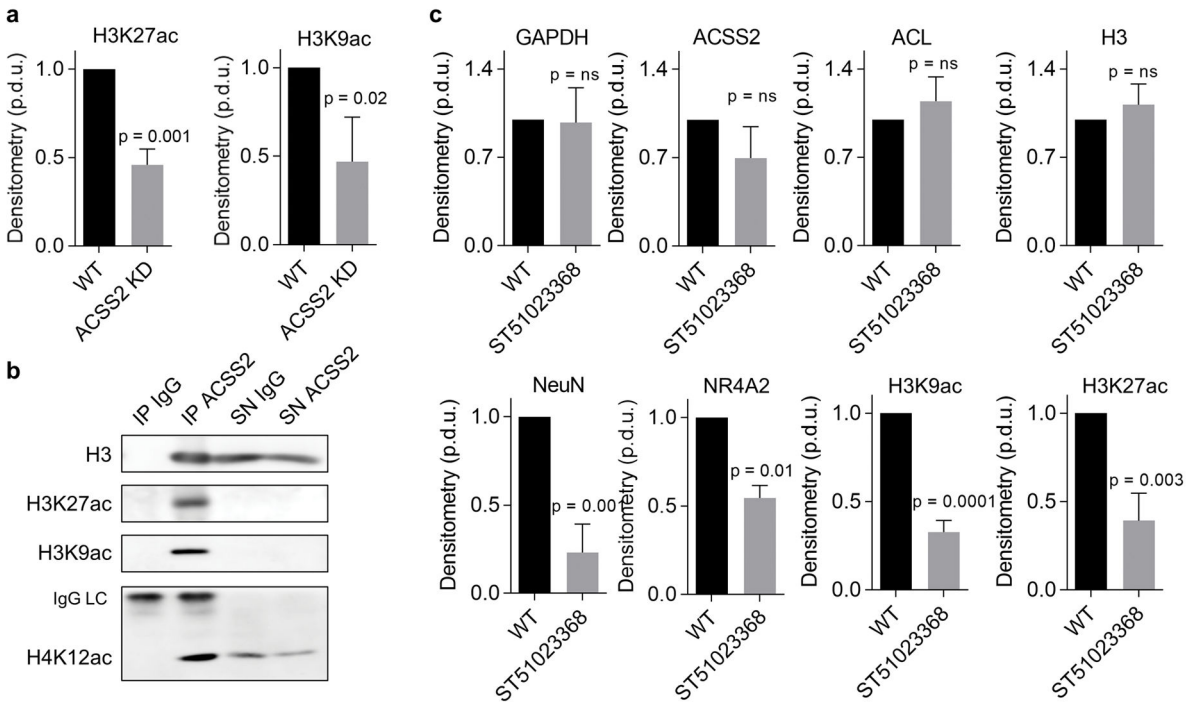


**Extended Data Figure 6.**

(a) Western blot analysis of whole cell lysates shows that lentiviral shRNA-mediated KD of ACSS2 lowers H3K9 and H3K27 acetylation (compare to Fig. 2g), quantified using ImageJ (n = 3, error bars: SE). (b) Western blot analysis of eluates and supernatants of IgG control and ACSS2 co-IP experiments indicates that ACSS2 binds to acetylated chromatin. (c) Western blots of lysates from primary hippocampal neurons (d7) treated for 24h with the ACSS2i, probed with the indicated antibodies (compare to Fig. 2j), and quantified using ImageJ (n = 3, error bars: SE).

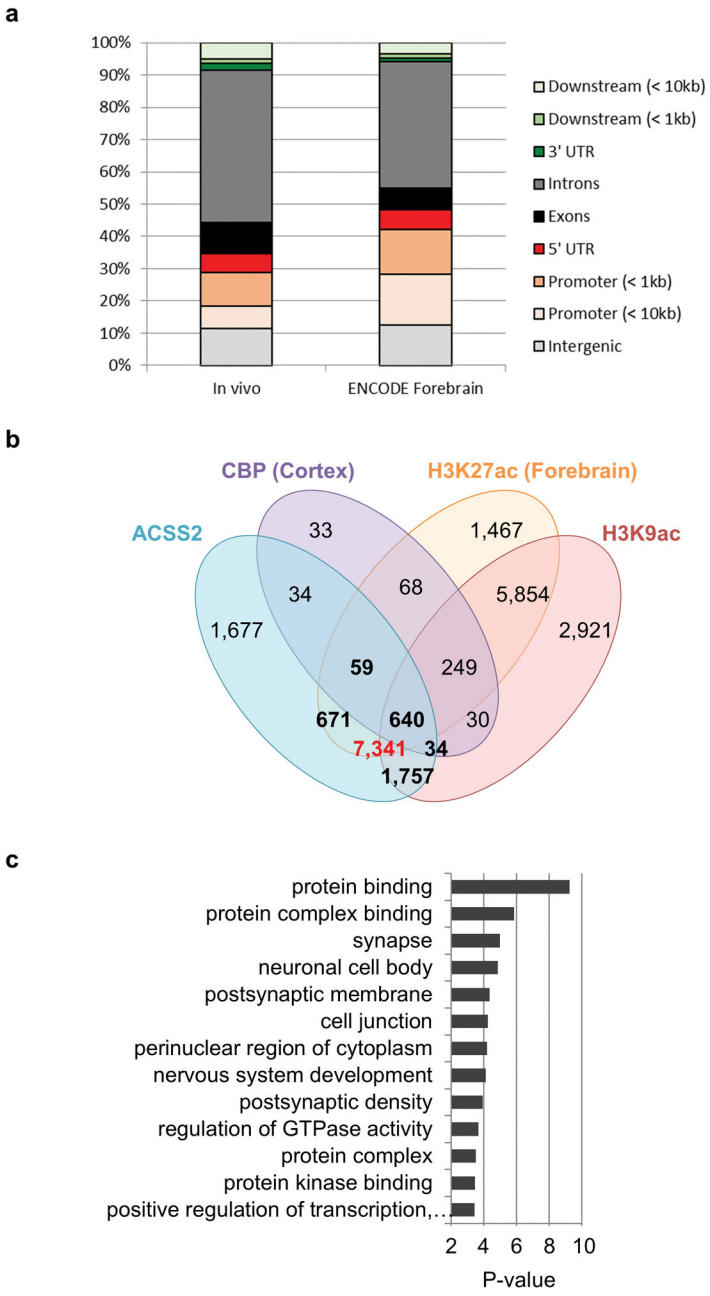


**Extended Data Figure 7.**

(a) Genome-wide compartment analysis of the *in vivo* hippocampal ChIP-seq of H3K9ac, and the mouse forebrain H3K9ac ChIP-seq from ENCODE, showing a similar peak distribution genome-wide: originating in different brain regions, the *in vivo* H3K9ac ChIP data are in strong agreement (Spearman R = 0.67) (b) Shown is a 4-way Venn diagram depicting overlap of RefSeq transcripts targeted by the indicated enzyme or modification (peaks for CBP (GSM1629373) and H3K27ac (GSM1629397) in mouse cortical neurons were called using MACS2 (narrow peaks, FDR 0.1%) with an input sonication efficiency control (GSM1629381); peaks were associated to the nearest TSS among all RefSeq

transcripts) (c) Gene Ontology enrichment analysis has been performed on common CBP:ACSS2 targets, indicating that these enzymes co-target genes that modulate synapse biology and synaptic membrane potential.

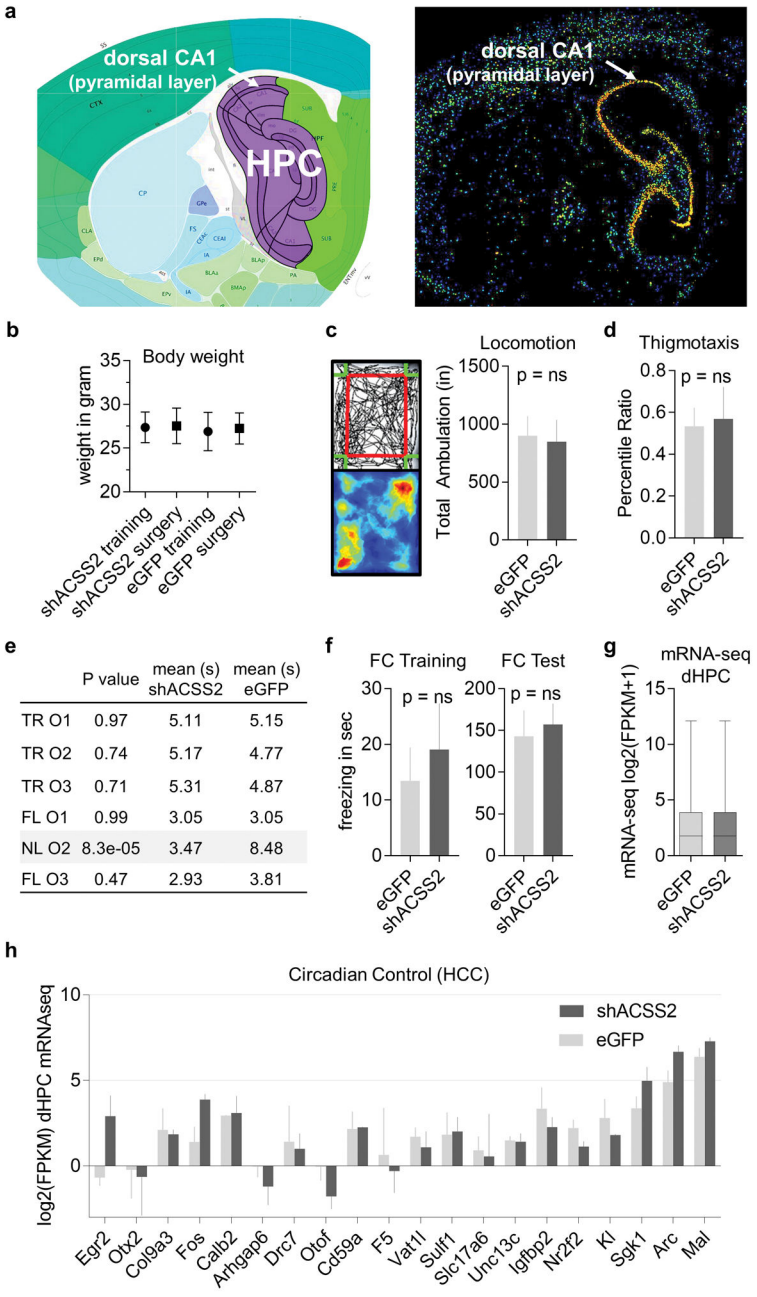


**Extended Data Figure 8.**

(a) ACSS2 RNA *in situ* hybridization on CA1 sagittal section ACSS2 (left: reference atlas, HPC – hippocampus proper; right: ACSS2 RNA in situ hybridization on HPC sagittal section, adapted from Allen Mouse Brain Atlas[12]). (b) Plot shows weight of eGFP-AAV9 control and shACSS2-AAV9 knockdown mice before intracranial surgery, and following

recovery before OLM task training (p = ns, n = 10 per group, error bars: SD). (c, d) ACSS2 knockdown animals showed no defect in locomotion or thigmotaxis (tendency to remain close to vertical surfaces in an open field, a measure of anxiety), as quantified over five minutes in the open field test; exemplary heatmap of tracking data shown in (c) (p = ns, n = 10 per group, error bars: SD). (e) Table of the exploration times by eGFP-AAV9 control and shACSS2-AAV9 knockdown mice recorded for the three objects (O1–3) during the first OLM training session (TR – Training) and the 24h retention test (NL – object in novel location, FM – objects remained in former location). (f) Compared to the control eGFP-AVV9 mice, ACSS2 knockdown mice show no defect in contextual fear memory. Freezing in FC chamber on day of contextual fear conditioning was recorded and quantified pre-shock (FC Training; p = ns, n = 10 per cohort, error bars: SD). Fear memory was measured as the freezing response after re-exposure to the context 1 day after contextual fear conditioning (aversive stimulus: 1.5 mA electrical shock; p = ns, n = 10 per cohort, error bars: SD). (g) RNA-seq was performed on the dorsal hippocampus of eGFP control and shACSS2 knockdown animals. Global transcript levels are not affected by ACSS2 knockdown (dHPC – dorsal hippocampus; four animals per group, two replicates for each condition, p = ns, Paired T test, error bars: SD) (h) Baseline expression of immediate-early genes in untrained animals is unaltered in ACSS2 KD mice. RNA-seq was performed on the dorsal HPC of eGFP control and shACSS2 KD animals ($r = 0.82$, $p < 0.0001$; HCC – homecage circadian control).

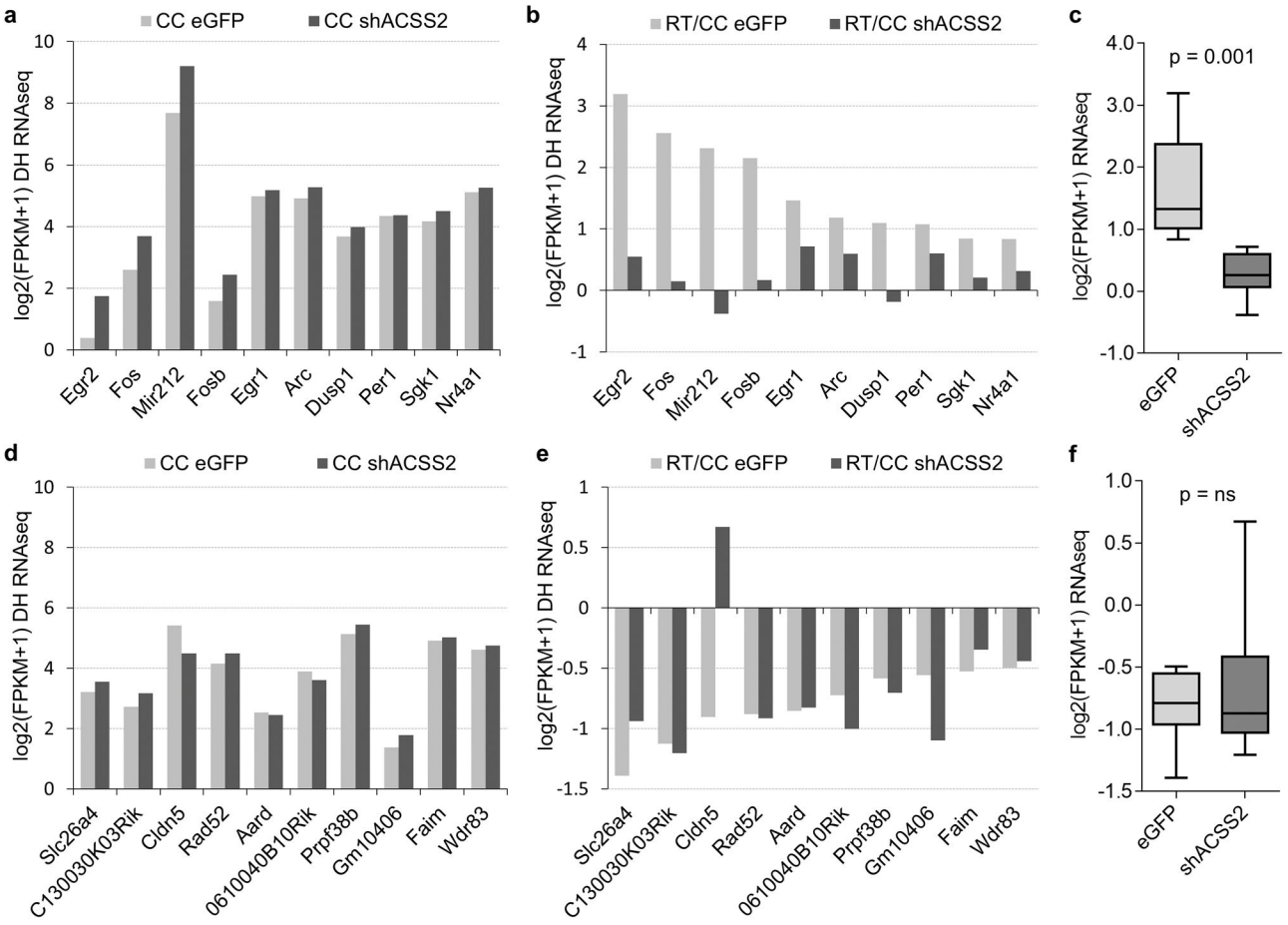


**Extended Data Figure 9.**

ACSS2 regulates retrieval-induced upregulation immediate-early genes *in vivo*. (a) Genome-wide RNA-seq was performed on the dorsal hippocampus of eGFP control and shACSS2 knockdown animals. The analysis was focused on the set of previously identified and validated genes that become upregulated during the sensitive period following memory retrieval. The baseline expression of immediate-early genes in untrained animals is not changed in shACSS2-AAV9 mice when compared to eGFP-AAV9 control mice (CC – circadian control). (b) During the sensitive period following contextual memory retrieval (RT – 30 min post-exposure to conditioning chamber 24h following fear conditioning), immediate-early genes are upregulated in dorsal HPC in the control injected animals. In contrast, the dynamic retrieval-induced expression of these early response genes is absent in ACSS2 knockdown animals ($p = 0.001$, Paired T test). (c) Boxplot shows the induction defect of immediate-early genes in shACSS2-AAV9 injected animals (RT/CC). (d) The baseline expression of genes that are downregulated following contextual memory retrieval is not altered in ACSS2 knockdown animals. (e) Downregulation of retrieval-responsive genes occurs both in eGFP control and ACSS2 knockdown mice, except Cldn5. (f) Boxplot compares retrieval-induced downregulation of retrieval-responsive genes in the dorsal hippocampus in eGFP control versus shACSS2 knockdown (RT/CC).

## Supplementary Material

Refer to Web version on PubMed Central for supplementary material.

## Acknowledgments

We thank the NeuronsRUs core of the Mahoney Institute for Neurological Sciences for preparations of primary hippocampal neurons. T.A. is supported by RO1 MH 087463. P.M. and S.L.B. are supported by NIH P01AG031862.

## References

1. Kandel ER, Dudai Y, Mayford MR. The molecular and systems biology of memory. Cell. 2014; 157:163–186. [PubMed: 24679534]
2. Zovkic IB, Guzman-Karlsson MC, Sweatt JD. Epigenetic regulation of memory formation and maintenance. Learn Mem. 2013; 20:61–74. [PubMed: 23322554]
3. Gräff J, Tsai LH. Histone acetylation: molecular mnemonics on the chromatin. Nat Rev Neurosci. 2013; 14:97–111. [PubMed: 23324667]
4. Wood, Ma, et al. Transgenic mice expressing a truncated form of CREB-binding protein (CBP) exhibit deficits in hippocampal synaptic plasticity and memory storage. Learn Mem. 2005; 12:111–119. [PubMed: 15805310]
5. Korzus E, Rosenfeld MG, Mayford M. CBP histone acetyltransferase activity is a critical component of memory consolidation. Neuron. 2004; 42:961–972. [PubMed: 15207240]
6. Kaelin WG, McKnight SL. Influence of metabolism on epigenetics and disease. Cell. 2013; 153:56–69. [PubMed: 23540690]
7. Katada S, Imhof A, Sassone-Corsi P. Connecting Threads: Epigenetics and Metabolism. Cell. 2012; 148:24–8. [PubMed: 22265398]
8. Cai L, Sutter BM, Li B, Tu BP. Acetyl-CoA induces cell growth and proliferation by promoting the acetylation of histones at growth genes. Mol Cell. 2011; 42:426–37. [PubMed: 21596309]
9. Wellen KE, et al. ATP-citrate lyase links cellular metabolism to histone acetylation. Science. 2009; 324:1076–80. [PubMed: 19461003]
10. Gut P, Verdin E. The nexus of chromatin regulation and intermediary metabolism. Nature. 2013; 502:489–98. [PubMed: 24153302]
11. Pietrocola F, Galluzzi L, Bravo-San Pedro JM, Madeo F, Kroemer G. Acetyl Coenzyme A: A Central Metabolite and Second Messenger. Cell Metab. 2015; 21:805–821. [PubMed: 26039447]
12. Lein ES, et al. Genome-wide atlas of gene expression in the adult mouse brain. Nature. 2007; 445:168–176. [PubMed: 17151600]
13. Qi Y, Wang JK, McMillian M, Chikaraishi DM. Characterization of a CNS cell line, CAD, in which morphological differentiation is initiated by serum deprivation. J Neurosci. 1997; 17:1217–1225. [PubMed: 9006967]
14. Comerford, Sa, et al. Acetate dependence of tumors. Cell. 2014; 159:1591–602. [PubMed: 25525877]
15. Sardi SP, Murtie J, Koirala S, Patten BA, Corfas G. Presenilin-Dependent ErbB4 Nuclear Signaling Regulates the Timing of Astrogenesis in the Developing Brain. Cell. 2006; 127:185–197. [PubMed: 17018285]
16. Peleg S, et al. Altered histone acetylation is associated with age-dependent memory impairment in mice. Science. 2010; 328:753–6. [PubMed: 20448184]
17. Aoyama T, et al. Histone modifiers, YY1 and p300, regulate the expression of cartilage-specific gene, chondromodulin-I, in mesenchymal stem cells. J Biol Chem. 2010; 285:29842–50. [PubMed: 20663886]
18. Vecsey CG, et al. Histone Deacetylase Inhibitors Enhance Memory and Synaptic Plasticity via CREB: CBP-Dependent Transcriptional Activation. J Neurosci. 2007; 27:6128–6140. [PubMed: 17553985]

19. Barrett RM, et al. Hippocampal focal knockout of CBP affects specific histone modifications, long-term potentiation, and long-term memory. Neuropsychopharmacology. 2011; 36:1545–56. [PubMed: 21508930]
20. Gräff J, Woldemichael BT, Berchtold D, Dewarrat G, Mansuy IM. Dynamic histone marks in the hippocampus and cortex facilitate memory consolidation. Nat Commun. 2012; 3:991. [PubMed: 22871810]
21. Ariyannur PS, et al. Nuclear-cytoplasmic localization of acetyl coenzyme a synthetase-1 in the rat brain. J Comp Neurol. 2010; 518:2952–77. [PubMed: 20533355]
22. Maren S, Holt W. The hippocampus and contextual memory retrieval in Pavlovian conditioning. Behav Brain Res. 2000; 110:97–108. [PubMed: 10802307]
23. Stanford SC. The Open Field Test: reinventing the wheel. J Psychopharmacol. 2007; 21:134–135. [PubMed: 17329288]
24. Balderas I, et al. The consolidation of object and context recognition memory involve different regions of the temporal lobe. Learn Mem. 2008; 15:618–624. [PubMed: 18723431]
25. Rogers JL, Hunsaker MR, Kesner RP. Effects of ventral and dorsal CA1 subregional lesions on trace fear conditioning. Neurobiol Learn Mem. 2006; 86:72–81. [PubMed: 16504548]
26. Peixoto LL, et al. Memory acquisition and retrieval impact different epigenetic processes that regulate gene expression. BMC Genomics. 2015; 16:S5.
27. Mamiya N, et al. Brain Region-Specific Gene Expression Activation Required for Reconsolidation and Extinction of Contextual Fear Memory. J Neurosci. 2009; 29:402–413. [PubMed: 19144840]
28. Poplawski SG, et al. Object-location training elicits an overlapping but temporally distinct transcriptional profile from contextual fear conditioning. Neurobiol Learn Mem. 2014; 116:90–5. [PubMed: 25242102]
29. Mashimo T, et al. Acetate Is a Bioenergetic Substrate for Human Glioblastoma and Brain Metastases. Cell. 2014; 159:1603–1614. [PubMed: 25525878]
30. Gao X, et al. Acetate functions as an epigenetic metabolite to promote lipid synthesis under hypoxia. Nat Commun. 2016; 7:11960. [PubMed: 27357947]
31. Mariño G, et al. Regulation of autophagy by cytosolic acetyl-coenzyme A. Mol Cell. 2014; 53:710–25. [PubMed: 24560926]
32. Takahashi H, McCaffery JM, Irizarry Ra, Boeke JD. Nucleocytosolic acetyl-coenzyme a synthetase is required for histone acetylation and global transcription. Mol Cell. 2006; 23:207–17. [PubMed: 16857587]
33. Walker DM, Cates HM, Heller EA, Nestler EJ. Regulation of chromatin states by drugs of abuse. Curr Opin Neurobiol. 2015; 30:112–121. [PubMed: 25486626]

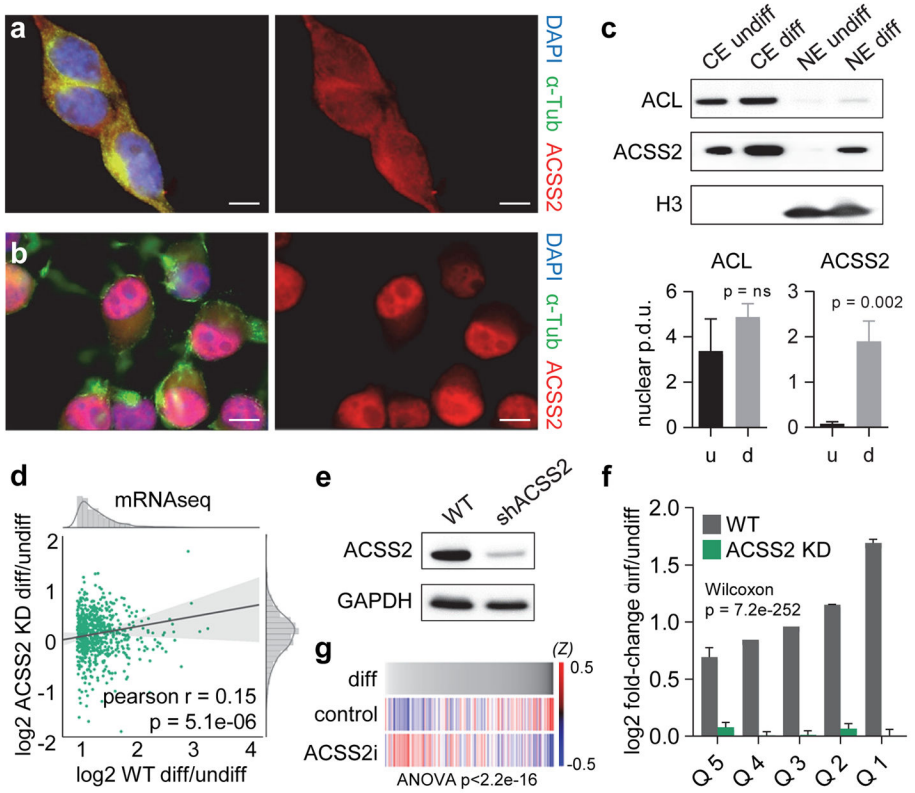


**Figure 1.**

Nuclear ACSS2 supports neuronal gene expression. (a) ACSS2 localizes to the cytoplasm in undifferentiated CAD neurons. ACSS2 was imaged by immunofluorescence microscopy in CAD cells (DAPI and α-Tubulin immunostaining visualize nuclei and cytoplasm, respectively). Scale bar = 10 μm (b) ACSS2 localizes to the nucleus of differentiated CAD neurons. (c) Western blot analysis of cytoplasmic (CE) and nuclear (NE) extracts from undifferentiated CAD cells (u) and differentiated CAD neurons (d) for ACSS2, ACL, and histone H3. Nuclear ACSS2 expression is increased upon differentiation (t test p = 0.002, n = 3, SD). (d) ACSS2 KD reduces differentiation-linked upregulation of neuronal gene expression program. Scatter plot contrasts the fold-change FPKM of induced genes (Extended Data Fig. 2c) between WT and ACSS2 KD (pearson r = 0.15, p = 5.1e-06). Marginal distributions show histogram and kernel density estimation. Ordinary least squares linear regression is displayed with 95% confidence interval. (e) Western blot of lysates from differentiated CAD neurons that were infected with lentiviral control (WT) or ACSS2 knockdown vector (shACSS2) (quantification shown in Extended Data Fig. 1g; n = 3). (f) ACSS2 KD greatly lowers gene upregulation. Quintiles of upregulated genes (red dots in Extended Data Fig. 2c) with the greatest fold-change increase in WT (grey). Corresponding gene quintiles depict fold-change FPKM in ACSS2 KD (green) (for each quintile, columns represent the mean induction value of genes, p = 7.2e-252, Wilcoxon rank-sum test, SE). (g) ACSS2i treatment in CAD neurons results in reduced expression of differentiation-induced genes. Plotted are all genes in order of fold-change in WT CAD differentiation, and z-scores were computed for ACSS2i-treatment and control, representing upregulation as blue and

downregulation as red (RNA-seq in 24h ACSS2i-treated and DMSO-control neurons, genes removed with z-score < 0.5).

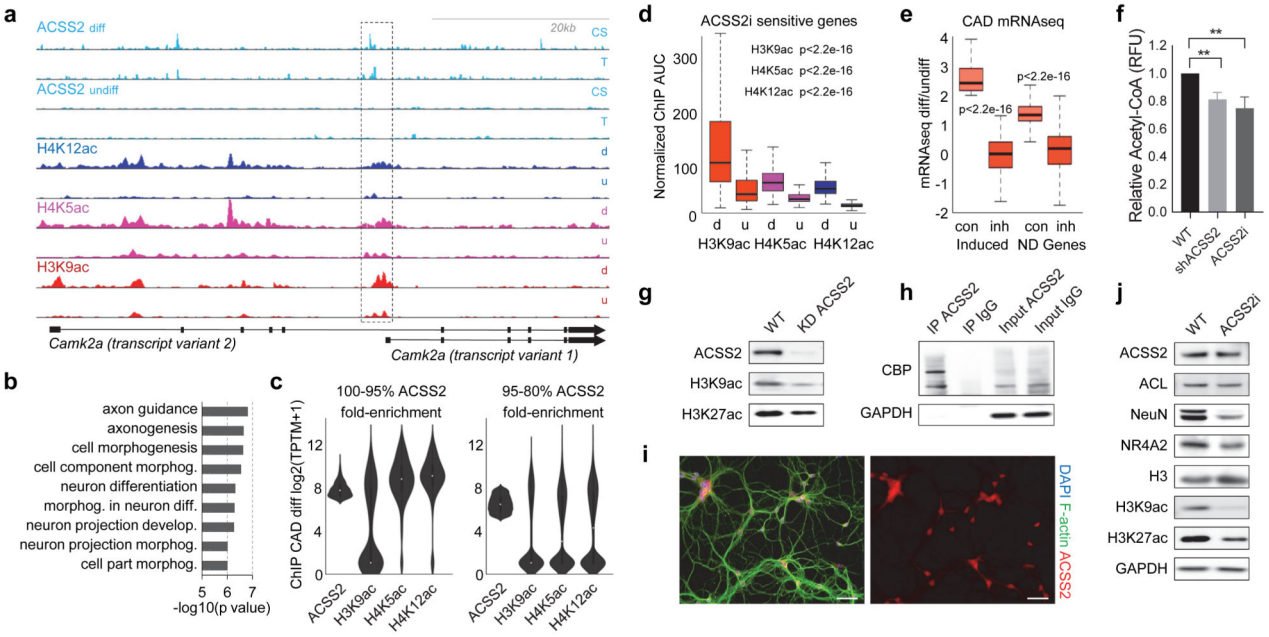


**Figure 2.**

ACSS2 is recruited to transcriptionally active chromatin and promotes neuronal histone acetylation. (a) Genome browser tracks showing ChIP-seq over the Camk2a locus shows that increases in H4K5, H4K12, and H3K9 acetylation co-occur with proximate ACSS2 enrichment upon CAD neuron differentiation (chr18: 60,920,000–60,990,000). (b) GO term enrichment analysis of top 5% genes that become ACSS2-bound in CAD neuron differentiation show neuronal pathways. (c) Violin-contour plots show ChIP-seq enrichment of the indicated histone acetylation occurs with top-ranked ACSS2 enrichment during CAD neuronal differentiation. (d) ChIP-seq enrichment of the 299 genes that are reduced upon ACSS2i treatment (details in methods) shows high correlation with histone acetylation in the differentiated state (d – differentiated, u – undifferentiated). (e) Analysis of all genes previously linked to neuronal differentiation (ND genes, AmiGO annotation set of 1,315 genes), and the subset of known ND genes that are induced in CAD cell differentiation (Induced), show reduced expression in ACSS2i-treated CAD neurons (inh) compared to DMSO control (con). (f) Nuclear acetyl-CoA levels are reduced in response to either KD of ACSS2 (mean $\Delta = -0.19 \pm 0.03$, $p = 0.003$) or application of the ACSS2 inhibitor (mean $\Delta = -0.25 \pm 0.05$, $p = 0.006$; $n = 3$, SD). (g) Western blot analysis of whole cell lysates shows that lentiviral shRNA-mediated KD of ACSS2 lowers H3K9 and H3K27 acetylation (quantifed in Extended Data Fig. 6a). (h) Western blot analysis of IP eluates shows that CBP is co-IPed in the ACSS2 IP, but not in the control IgG IP. (i) Immunofluorescence in primary hippocampal neurons shows nuclear localization of ACSS2 (day 7 of *in vitro* differentiation culture, isolated from C57BL/6 embryos). Scale bar = 50 μm (j) Western blots of lysates from primary hippocampal neurons (d7) treated for 24h with the ACSS2i, probed with the indicated antibodies (quantified in Extended Data Fig. 6c) shows reduction of histone acetylation.

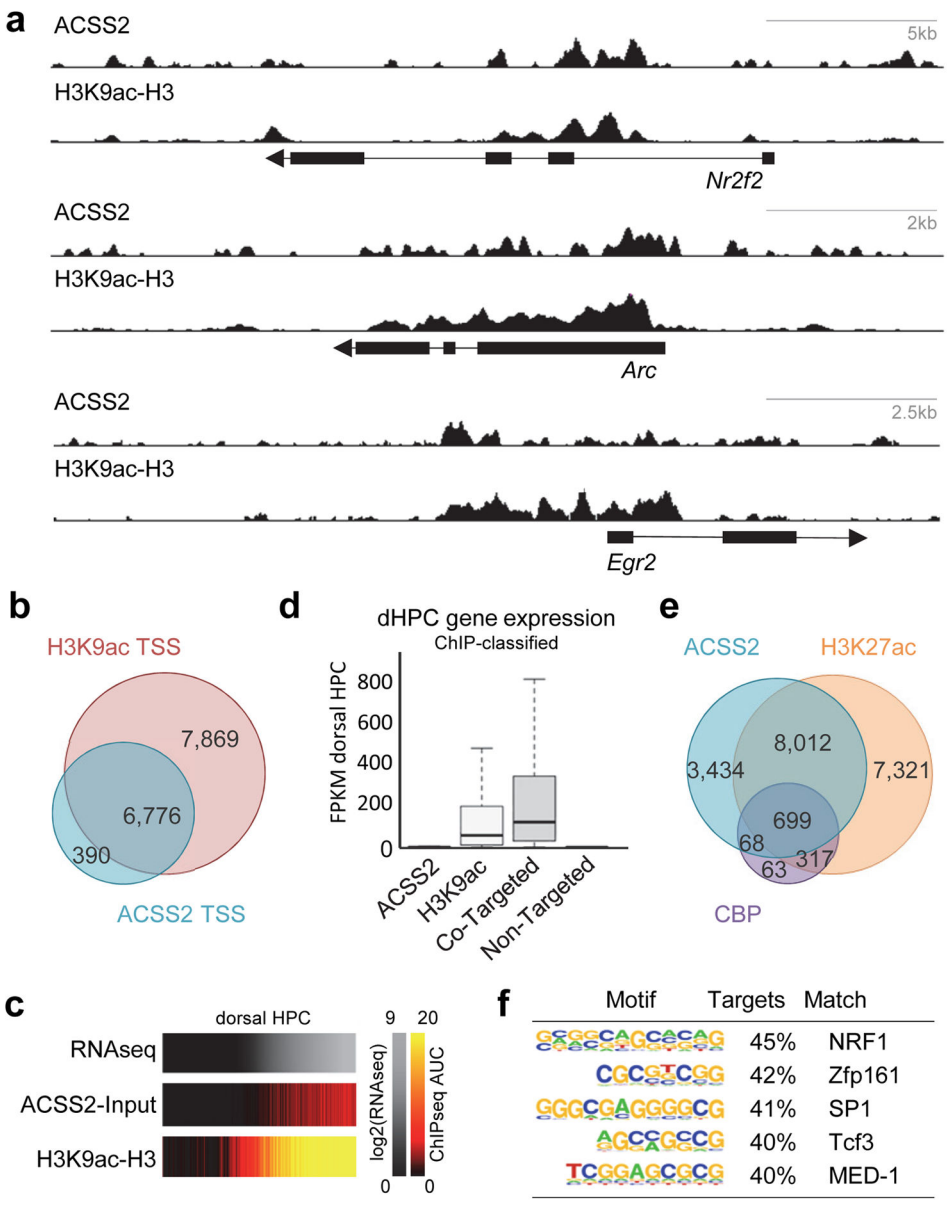


**Figure 3.**

ACSS2 ChIP-seq localization is linked to histone acetylation *in vivo* in mouse hippocampus (HPC). (a) ChIP-seq for ACSS2 and H3K9ac in mouse HPC. Track-views show ACSS2 and H3K9ac for three canonical neuronal genes involved in memory: Arc, Egr2, and Nr2f2 (chr15:74496025–74506488, chr10:66991018–67006804, and chr7:77488549–77516626, respectively). (b) Venn diagram shows *in vivo* HPC ACSS2 and H3K9ac peaks co-localize with the nearest gene TSS (< 1kb from peak) among all RefSeq transcripts. (c) RNA-seq expression in dorsal HPC correlates with ACSS2 binding and enrichment of H3K9 acetylation. (d) Expression profile of genes classified by way of their ACSS2 and H3K9ac enrichment state (d) Venn diagram shows the overlap between ACSS2 targeted genes (HPC), and CBP and H3K27ac enrichment for entire set of peaks (ENCODE CBP and H3K27ac ChIP-seq in mouse forebrain and cortex). (e) RNA expression heat map in HPC showing co-

enrichment of ACSS2 and H3K9ac. (f) Motif analysis at ACSS2 peaks from *in vivo* ChIP-seq in HPC showing top enrichment of NRF1, a neuronal transcription factor.

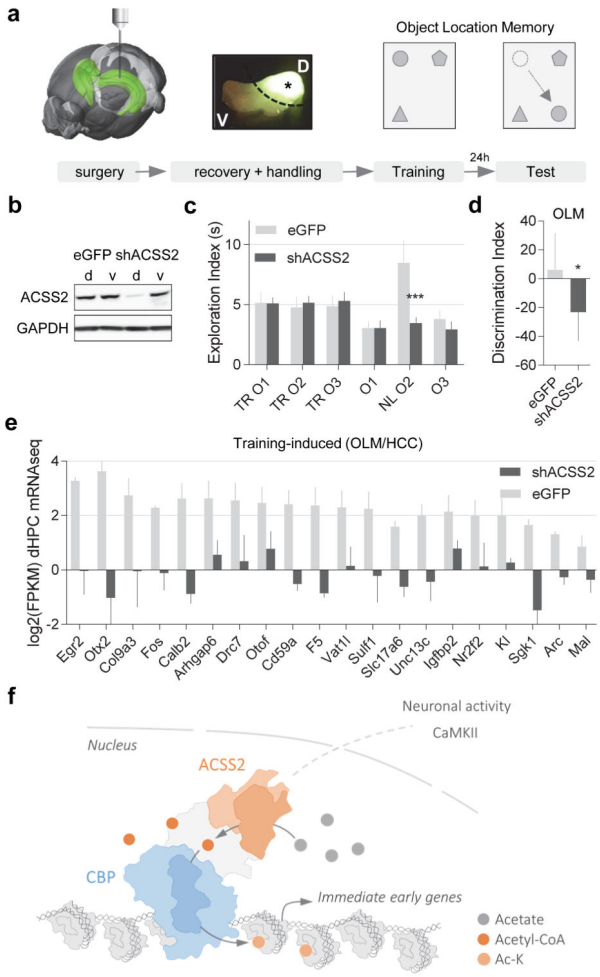


**Figure 4.**

ACSS2 knockdown in dorsal HPC impairs object location memory (OLM) and upregulation of immediate-early genes following training. (a) Stereotactic surgery was performed to deliver AAV9 knockdown vector into the dorsal HPC (AP, −2.0mm; DV, −1.4mm; ML, +/−1.5mm from Bregma); four weeks later habituated mice received training for object location memory (four 5 min training sessions in arena with three different objects). 24 hours later the mice were given a retention test in which one object was moved to a novel location (n = 10 per cohort). (b) Western blot analysis of HPC tissue harvested from animals injected dorsally with either eGFP control or ACSS2 KD vector (d – dorsal, v – ventral) shows specific reduction of ACSS2 in dorsal HPC. (c) ACSS2 KD animals are impaired in object location memory. eGFP-control and shACSS2-AAV9 mice display no preference for any of three objects (O1–3) during the OLM training session (TR – Training). In the 24h retention test, eGFP-AAV9 control mice show preference for novel object location (NL), whereas the shACSS2 KD mice display no preference for the novel object location (NL). (d) The spatial memory defect in ACSS2 KD animals manifests in lowered discrimination index (% DI = (t NL − t FL)/(t NL+ t FL)) compared to control mice (ΔDI = −29.5 ± 11.4, p = 0.02; n = 10, SD). (e) Training-induced expression of a cohort of immediate-early genes (see Extended Data Fig. 8h) is greatly attenuated in ACSS2 KD animals (four animals per group,

two replicates for each condition, $p < 0.0001$, Paired T test, SD). (f) Model for ACSS2 functioning as a chromatin-bound coactivator to locally provide acetyl-CoA to promote histone acetylation and activity-induced upregulation of immediate-early genes.